CHALMERS
UNIVERSITY OF TECHNOLOGY

Studies on electron transfer and recombination across dye-TiO_2-SnO_2-acceptor assemblies

Master's thesis in the Materials Chemistry programme

ELIN SUNDIN

Department of Chemistry and Chemical Engineering
CHALMERS UNIVERSITY OF TECHNOLOGY
Gothenburg, Sweden 2016

MASTER'S THESIS

Studies on electron transfer and recombination across dye-TiO_2-SnO_2-acceptor assemblies

Department of Chemistry and Chemical Engineering
Division of Physical Chemistry
CHALMERS UNIVERSITY OF TECHNOLOGY
Göteborg, Sweden

Studies on electron transfer and recombination across dye-TiO_2-SnO_2-acceptor assemblies
ELIN SUNDIN

Supervisor: Valeria Saavedra, Chalmers University of Technology
Examiner: Maria Abrahamsson, Chalmers University of Technology
Department of Chemistry and Chemical Engineering
Division of Physical Chemistry
Chalmers University of Technology
SE-412 96 Göteborg
Sweden
Telephone: + 46 (0)31-772 1000

Göteborg, Sweden

Studies on electron transfer and recombination across dye-TiO_2-SnO_2-acceptor assemblies

Department of Chemistry and Chemical Engineering
Division of Physical Chemistry
Chalmers University of Technology

Abstract

As the effects of global warming becomes more apparent, the demand for new renewable energy sources increases. The sun is an almost endless source of energy that is not used to its full potential due to the lack of storing possibilities. One way of storing the solar energy could be to produce solar fuels. However, producing solar fuels requires multiple electron transfer (MET), which is difficult in molecular systems. Using hybrid molecular-inorganic systems could overcome this problem by making the systems more stable. In this project we have studied the electron transfer across the interface between semiconductors and an acceptor molecule, Protoporphyrin IX cobalt (CoPPIX). The results demonstrate that CoPPIX can be reduced via conduction band mediated electron transfer on both of the semiconductors, suggesting that it is possible to use these systems for solar fuel production. In this project we have also investigated the possibility to achieve a longer lived charge separated state in hybrid-molecular assemblies, these systems consists of a dye, a semiconductor and an acceptor molecule. The effect of using two semiconductors, titanium(IV) oxide (TiO_2) and tin(IV) oxide (SnO_2), instead of one has been examined together with the dye D35 and CoPPIX as the acceptor molecule. The results from this study suggests that the combined TiO_2/SnO_2 system has a similar recombination rate as the system with only TiO_2, and that the charge separated state has the shortest lifetime on SnO_2. The lifetime of the charge separated state is increased the most by adding the acceptor molecule to the system, suggesting that electrons get transferred from the dye to the acceptor via the conduction band of the semiconductors.

Key words: solar fuels, conduction band mediation, dye sensitized, multiple electron transfer

List off abbreviations

A – acceptor

CB – conduction band

CE – counter electrode

CoPPIX – protoporphyrin IX cobalt

CV – cyclic voltammetry

D – donor

D35 - (E)-3-(5-(4-(bis(2',4'-dibutoxy-[1,1'-biphenyl]-4-yl)amino)phenyl)thiophen-2-yl)-2cyanoacrylic acid

DMSO – dimethyl sulfoxide

IC – internal conversion

ISC – intersystem crossing

MeCN – acetonitrile

MeOH – methanol

MET – multiple electron transfer

PEG – polyethylene glycol

PEO – polyethylene oxide

RE – reference electrode

SnO_2 – tin(IV) oxide

TAS – transient absorption spectroscopy

$TBAPF_6$ – tetrabutylammonium hexaflourophosphate

TiO_2 – titanium(IV) oxide

VB – valence band

VR – vibrational relaxation

WE – working electrode

Table of Contents

1. Introduction

Global warming, which is caused to a large extent by the burning of fossil fuels, is a concern in today's society and there is a strong need for new renewable energy sources. The sun is a great source of energy, the radiation from it contains about 5000 times more energy than the global energy demand, and using it more efficiently would therefore decrease the emissions and the global warming (1). Today, the energy from the sun is mostly used to produce electricity without the ability of storing it. One way of using the energy from the sun more efficiently in the future, with the ability of storing it, could be to produce solar fuels. These could be made from reduction of carbon dioxide (CO_2) to produce for example methane (CH_4) (2). The concentration of CO_2 in the atmosphere has increased with about 40 % since the pre-industrial era, and solar fuels that could recycle this CO_2 into usable fuel is therefore very attractive (3). The resulting fuels from reduction of CO_2 are furthermore based on hydrocarbons and could easily be integrated into the current energy and transport systems.

1.1. Background

The principle for solar fuel production is to make use of the energy in the radiation from the sun, and by photocatalysis reduce a low value substrate into a useful fuel. There are different approaches how to collect and use the energy from the sun, for example the molecular approach and the inorganic approach, but the principle is the same for all approaches. Energy from the sun is harvested and used to achieve charge separation, i.e. separation of electrons and holes in the systems. The electrons are then used to drive chemical reactions where a cheap substrate is converted into a useful fuel via a reduction reaction. The substrate that is reduced can be CO_2 or H^+, yielding either for example methane (CH_4) or hydrogen gas (H_2). Oxidation of water is the best option for filling the holes in these systems, since it is an electron source in abundance on earth. (2)

When producing solar fuels from reduction of CO_2, multiple electron transfer (MET) is necessary. Photoreduction of CO_2 with one electron requires absorption of a single photon which leads to a single charge separation, the product formed, $CO_2^{\bullet -}$, is however unstable, not useful as a fuel and will decompose immediately after it has been formed. The reaction is also thermodynamically unfavorable and has a very negative potential (4). To produce methanol or methane, six or eight electrons needs to be moved simultaneously and MET is therefore required, see table 1.1 (5). Also for the reduction of H^+ to H_2 two electrons are necessary, so a part of the research in producing solar fuels is therefore focused on how to induce MET (6), (2).

Table 1.1. Reduction potentials of CO_2 vs NHE at pH 7 (5).

Reaction	Potential vs NHE in pH 7
$CO_2 + e^- \rightarrow CO_2^{\bullet -}$	-1.90 V
$CO_2 + 2H^+ + 2e^- \rightarrow CO + H_2O$	-0.53 V
$CO_2 + 2H^+ + 2e^- \rightarrow HCO_2H$	-0.61 V
$CO_2 + 4H^+ + 4e^- \rightarrow HCHO + H_2O$	-0.48 V
$CO_2 + 6H^+ + 6e^- \rightarrow CH_3OH + H_2O$	-0.38 V
$CO_2 + 8H^+ + 8e^- \rightarrow CH_4 + 2H_2O$	-0.24 V

The molecular approach for solar fuel conversion is mostly inspired by the photosynthesis. The goal is to design a molecular system that can harvest energy from the sun and produce a fuel from that energy and water, this is called artificial photosynthesis (7). When using a molecular approach, different components are needed, either incorporated into a large molecule or as separated parts; a

photosensitizer (P) that can harvest the light and move electrons to an acceptor (A), and a donor (D) that can give the electrons back to the photosensitizer. A schematic illustration of a molecular approach for solar fuel conversion is shown in figure 1.1. (2) The molecular systems can be very selective, but despite massive research they are still very unstable with a short lifetime and low turnover numbers (8).

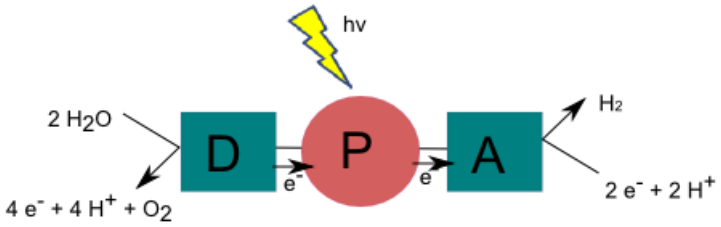

Figure 1.1. Schematic picture of a molecular approach for solar fuel production for H_2-production. This figure is adapted from reference (2).

Another approach for producing solar fuels is the inorganic approach. In this approach, semi-conductors are often used to absorb the energy from the sun which leads to a separation of electrons and holes. The potential that is created can then be used to drive the reduction reactions at the interfaces, this is called a photoelectrochemical cell. A schematic picture of a photoelectrochemical cell is shown in figure 1.2. Systems like this are stable with the possibility to induce MET reactions, but they are not as selective as the molecular approaches and can typically only absorb the UV-light from the sun. (9)

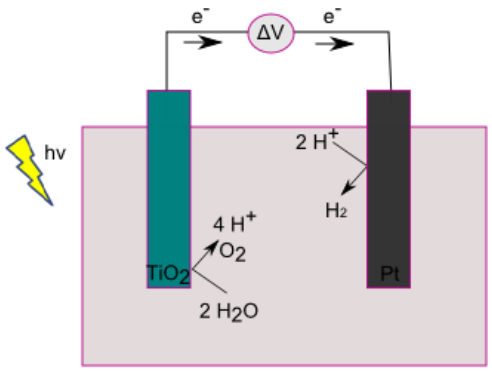

Figure 1.2. Schematic picture of a photoelectrochemical cell which is an inorganic approach for solar fuel production. The figure is adapted from reference (9).

One way to take advantage of the benefits of both the molecular and inorganic approaches and easier induce MET reactions while still having a selective system, is to construct hybrid systems. In these systems, the conduction band (CB) of semiconductors can work as a redox pool for the electrons, so that they later can be used in chemical reactions taking place at the surface of the nanoporous semiconductor. Since the band gap between the valence band (VB) and the CB in semiconductors like titanium(IV) oxide (TiO_2) only can absorb energy in the UV-region, a photosensitizer (dye) is attached to the semiconductor to also take advantage of the visible light. The dye can absorb energy in the visible region and become excited, the electrons that are excited can then be injected to the CB of the semiconductor. A molecular catalyst should then accept the electrons from the CB, and use them to drive for example the reduction reactions from CO_2 to CH_4. (2), (10)

In order to have a natural driving force for the electron transfer to the anchored catalyst, the potential of the catalyst needs to be less negative than the CB of the semiconductor. A competing reaction that could lower the efficiencies in the hybrid systems is the interfacial recombination, when electrons instead of being transferred to the catalyst recombine back to the dye. It is therefore important to minimize the recombination rate to the dye in order to achieve a long lived charge separated state (10).

1.2. Purpose of the project

There are two main purposes of this project. The first is to demonstrate conduction band mediated electron transfer from semiconductors to an acceptor molecule. The second purpose is to evaluate the possibility to achieve a longer lived charge separate state between the dye and the semiconductor in hybrid dye-semiconductor assemblies by using two different semiconductors, TiO_2 and tin(IV) oxide (SnO_2). As illustrated in figure 1.3, TiO_2 has a more negative potential than SnO_2, this difference in potential creates a driving force for the electron transfer between the CB of TiO_2 to the CB of SnO_2. If an acceptor molecule (model catalyst) with a lower potential also is incorporated into the system, the driving force for the electron transfer will be towards that molecule. Electron transfer that occurs stepwise like this is called multistep electron transfer (11) or an electron transfer cascade (12). This is what occurs naturally in the photosynthesis and has been proven to be more efficient with a longer lived charge separated state than if electrons are transferred in only one step (11), (12). This is due to the physical barrier that is created when electrons are transferred stepwise. If electrons are transferred from the dye to TiO_2 and then to SnO_2, there will be a barrier for the transfer back to the dye. This since the electrons then need to pass a higher energy level, which is energetically unfavorable (13). In this project an organic dye called D35 is used as the dye and Protoporphyrin IX cobalt (CoPPIX) is used as the model catalyst and electron acceptor.

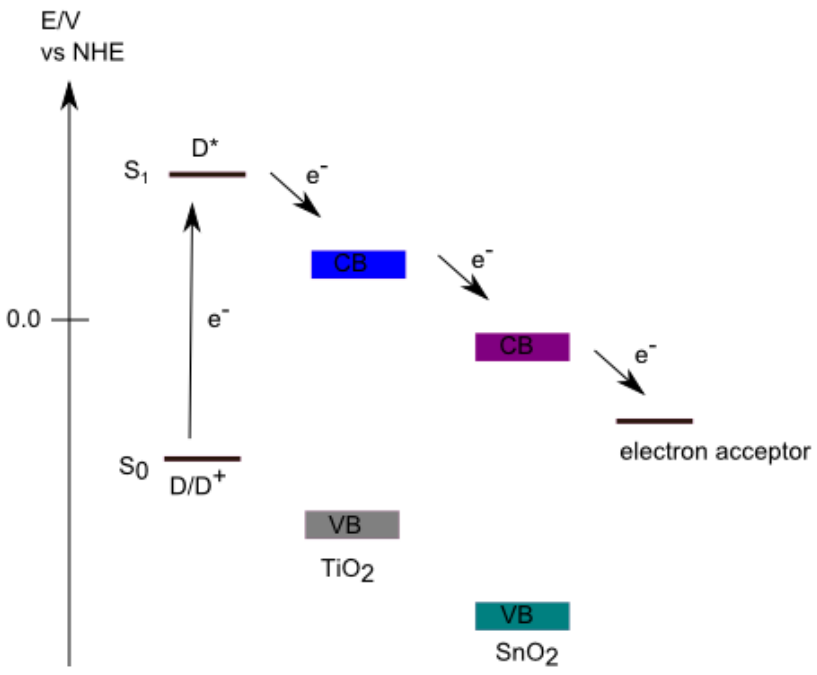

Figure 1.3. Schematic picture of the system with dye, semiconductors and acceptor that is used in this project.

2. Theory

2.1. Energy levels of molecules

To describe chemical systems and light-matter interactions, one has to make use of quantum mechanics. Quantum mechanics describes electrons as both particles and waves simultaneously and the energetic positions of the electrons in atoms and molecules are described by the atomic and molecular orbitals. These orbitals are situated at different energy levels, and electrons start to fill the orbitals with the lowest energy first. Two electrons with opposite spin can occupy the same orbital and if orbitals have the same energy, the electrons first occupy them one by one. In figure 2.1, the energy levels of the orbitals in the H_2-molecule is illustrated. (14)

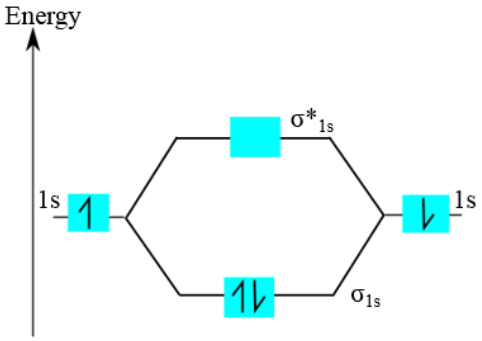

Figure 2.1. Illustration of the energy levels in a hydrogen molecule, the sigma bonding orbital (σ) is occupied while the antibonding sigma orbital (σ) is unoccupied.*

More unpaired electrons leads to higher multiplicity; if all electrons are in pairs it is called a singlet state (S) and if two electrons are unpaired it is called a triplet state (T). The highest occupied orbital (HOMO) is the orbital with the highest energy that is occupied in the ground state, and the lowest unoccupied orbital (LUMO) represents the first excited state. (14)

2.1.1. Light-matter interactions

Light can interact with matter and charged particles in molecules. If the energy in the light equals the difference in energy between two orbitals, the light can be absorbed and the molecule becomes excited. It is the light in the UV- and visible region that has the suitable energy to produce these electronic transition in molecules. Jablonski diagrams are often used to describe the different electronic transitions and the possible de-excitation pathways in molecules. A Jablonski diagram is presented in figure 2.2 below. Absorption of a photon leads to population of a higher energy orbital. Quickly after excitation, non-radiative vibrational relaxation (VR) takes place to the lowest vibrational state of the excited state. Fluorescence is a radiative emission that occurs from transitions between different singlet states and phosphorescence is a much slower radiative emission that comes from transitions between states of different multiplicity. There are also other non-radiative transitions, internal conversion (IC) and intersystem crossing (ISC) that does not change the total energy of the molecule. (14)

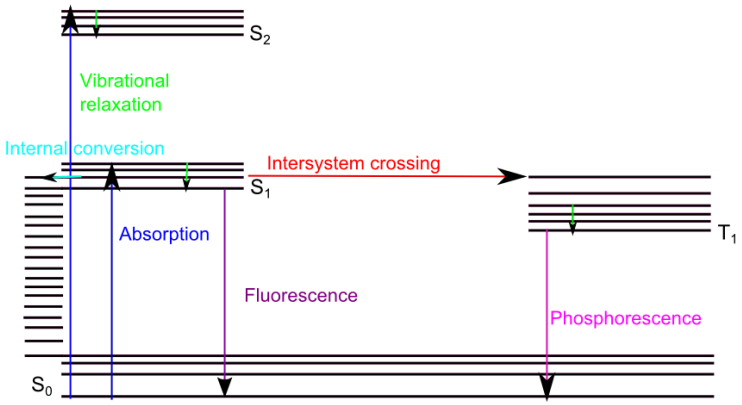

Figure 2.2. Jablonski diagram with arrows indicating absorption, fluorescence, phosphorescence, vibrational relaxation, internal conversion and intersystem crossing.

It is the distribution of states that gives the absorption and emission spectrum of molecules. According to *Kasha's rule* emission occurs from the lowest vibrational state. The emission and absorption spectra is therefore not equal and this difference is called the *Stokes shift*. (15)

The excited state returns to the ground state after some time. The mean lifetime of the excited state, τ, can be described as a first order decay corresponding to three unimolecular processes for the deactivation. These processes are the different de-excitation pathways, the lifetime is the reciprocal of the sum of the rate constants for the different processes, as described in equation 1 below (16):

$$\tau = \frac{1}{k_r + k_{nr} + k_p} \tag{1}$$

Where k_r and k_{nr} is the rate constant for the radiative and non-radiative deactivation respectively, and k_p the rate constant for the chemical processes for deactivation. The quantum yield is used to describe the efficiency of a photoinduced process, it is defined as the number of photons taking a specific track divided by the photons that are absorbed (16). The quantum yield for fluorescence can be written as equation 2 below, where k_r is the rate constant for the radiative processes and k_{nr} the rate constant for the non-radiative processes (17). When the quantum yield decreases it is called quenching. This can happen for many reasons, for example from collisions with other molecules or from electron transfer (15).

$$\Phi_F = \frac{k_r}{k_r + k_{nr}} \tag{2}$$

2.1.2. Photoinduced electron transfer

Photoinduced electron transfer, as presented in equation 3, is when electrons are transferred from a donor to an acceptor while one of them is in a photoexcited state. The donor and acceptor can either be within the same molecule or be separate molecules. The electron transfer creates a charge separated state between electrons and holes in the system. From the redox potentials of the states of the involved molecules, the direction of the electron transfer is decided. (15)

$$D|A \rightarrow D^*A \rightarrow D^+|A^- \tag{3}$$

Marcus theory is often used to explain photoinduced electron transfer. Here the potential energy of the surfaces of the charge separated state $D^+|A^-$ and the D-A complex is described by parabolic functions. To reach the charge separated state, the excited D*|A complex needs to move through a transition state that is situated where the two surfaces meet. For this to happen, the necessary activation energy ($\Delta G^{\#}$) needs to be provided. When the charge separated state has been created, the complex reorganize until equilibrium is reached and then releases energy called the reorganization energy (λ). The kinetics for the electron transfer can be described by equation 4 below. (10)

$$k_{ET} = \left(\frac{\pi}{\hbar^2 k_B T}\right)^{1/2} |V_{DA}| \exp - \left(\frac{(\lambda + \Delta G^0)^2}{4\lambda k_B T}\right) \quad (4)$$

Where $\hbar$ is the reduced Planck constant, k_B is Boltzmanns constant, T is the temperature, V_{DA} is the coupling between the donor and acceptor, ΔG^0 is the driving force and λ is the reorganization energy. There are three different regions according to this theory (see figure 2.3 below) (10):

1. The first region is where $\lambda > \Delta G^0$, here the rate of the electron transfer increases with increased driving force, this is called the normal region.
2. The second region is where $\lambda = \Delta G^0$, here there is no activation energy needed for the reaction.
3. The third region is the inverted region where $\lambda < \Delta G^0$, here the rate of the reaction decreases with increased driving force.

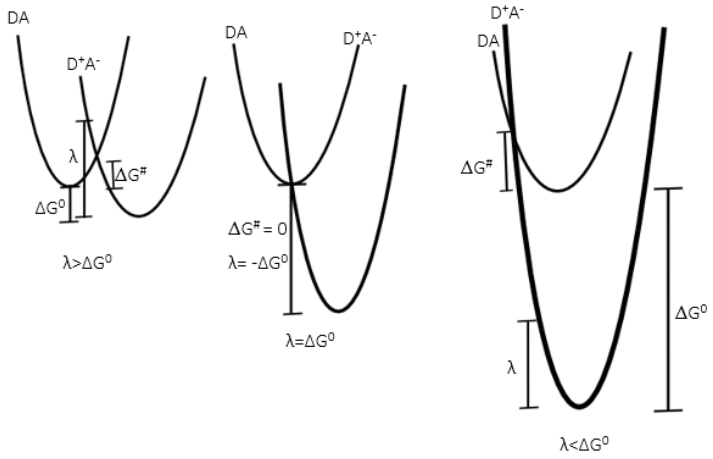

Figure 2.3. Schematic picture of the different regions in Marcus theory, leftt: normal region, middle: activationless region and right: inverted region

The photoinduced electron transfer reactions that are of interest in this project are the transfer of electrons from the excited dye to the CB of the semiconductors and the transfer of electrons to the acceptor from the CB of the semiconductors.

2.2. Semiconductors

Semiconductors are materials that are insulating in their ground state but can conduct electricity under certain conditions. The electrons in semiconductors are said to be situated in bands instead of orbitals because of the many available states with similar energy. The bands are thus combinations of the different orbitals with similar energy. Semiconductors have a filled VB and an unfilled CB in the ground state. The band gap can usually absorb energy from light in the UV-region which makes the material conductive (18). When the CB gets filled with electrons, these electrons can be seen in the absorption spectrum as a broad absorption above 600 nm (19).

The CB can also be occupied by electrons via photoinduced electron transfer when a photosensitizer (dye) is chemically attached to the surface of the semiconductor. Electrons are injected from the dye to the CB when the dye is in an excited state. For the injection of electrons to be efficient, there needs to enough electronic coupling between the dye and the semiconductor (20). The injection reaction is spontaneous if the energy of the excited dye is more negative than the CB potential of the semiconductor. The injection of electrons must be faster than the decay from the excited state to the ground state of the dye in order for this process to be efficient (21).

2.2.1. Dye sensitized solar cells with TiO_2 and SnO_2

Dye-sensitized solar cells consist of a film of a mesoporous semiconductor with a monolayer of a dye in a solution of a redox electrolyte. When the sun is illuminating the device, the dye absorbs energy and becomes excited to a higher energy level, the excited electrons are then injected to the CB of the semiconductor via photoinduced electron transfer. These electrons are then transferred to an external circuit and the current is collected, the electrolyte then regenerates the dye and the process can start over (22). The electrons could instead of being transferred to the circuit recombine back to the dye, this however is a slow process that does not affect the efficiency of these devices much (23). The principle of dye sensitized solar cells could also be used in hybrid systems for solar fuel production in the future, then the recombination of electrons to the dye would be the main competitive route (10). The reason for this will be further discussed in section 2.3.3.

TiO_2 is a well-studied semiconductor with many different applications. It is the most commonly used semiconductor for dye sensitized solar cells (22), and is also used in photocatalytic applications (24). TiO_2 is found in three main structures; rutile, anatase and brookite (25). For films used in dye-sensitized solar cells, anatase is the most commonly structure used (22). Anatase has a band gap of 3.2 eV (25).

SnO_2 has a lower CB potential than TiO_2 and has been studied as a potential semiconductor for dye sensitized solar cells. SnO_2 has a higher electrical conductivity and electron mobility than TiO_2 and is therefore a promising option in these devices, it has however shown lower efficiencies (26). Attempts have been done to try to combine TiO_2 with SnO_2 since the difference in potentials should make charge separation easier while suppressing recombination. These attempts has resulted in slower recombination rate (26) (27) (28).

2.2.2. Conduction band mediated electron transfer

When there is an overlap between the reduction potential of an anchored acceptor molecule and the CB edge of semiconductors, electrons can be transferred to that molecule. This is called conduction band mediation. The CB can in this way hold electrons, so that they later could be transferred to an anchored catalyst and used in chemical reactions taking place at the surface (29). The CB potential of TiO_2 is around -0.6 V vs NHE at pH 7 and the CB of SnO_2 has been reported to be about 0.5 V more positive than that, so an acceptor molecule needs to have a lower reduction potential than 0.1 in order to efficiently accept electrons from SnO_2 (30).

Conduction band mediation was first proved for a ruthenium complex, $[Ru(bpy)_2(deebq)](PF_6)_2$[1], and iron protoporphyrin IX (hemin) on a TiO_2 surface by Staniszewski and co-workers. They showed that it is possible to have a fast reduction of a substrate while the oxidation is slow, if the CB edge is at the right energy level and overlaps with the energy level of the reduced species. The CB edge of TiO_2 with respect to $[Ru(bpy)_2(deebq)](PF_6)_2$ and hemin are illustrated in figure 2.4 below. Because the CB

[1] bpy=2-2'-bipyridine, deebq= 4,4'-diethylester-2,2'-biquinoline

potential only overlaps with the reduction and not the oxidation of hemin, the reduction is fast while the oxidation is slow. For the ruthenium complex, the overlap is with both the oxidized and the reduced state, and therefore both oxidation and reduction is fast. (29)

These results indicate that it is possible to transfer electrons via the CB to an acceptor molecule, and that these electrons does not return to the semiconductor. It is possible to tune the CB edge by using different small cations in the electrolyte. The small ions can be situated close to the surface due to their small size, and can in that way interact with the surface energy levels. Also acceptor molecules with reduction potentials that not is at the exact right value could therefore be used. (29)

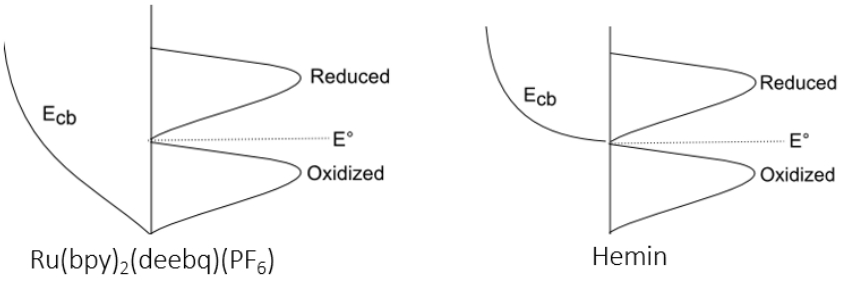

Figure 2.4. CB edge for TiO_2 with $[Ru(bpy)_2(deebq)](PF_6)_2$ and hemin on the surface. Both oxidation and reduction are fast for the ruthenium complex since both of the states overlap with the CB edge. Fast reduction and slow oxidation is observed for hemin since only overlap with the reduced stag. The figure is adapted from reference (29).

2.3. Dye-semiconductor-acceptor assemblies for photocatalysis

In figure 2.5, a schematic picture of a hybrid system that uses conduction band mediated electron transfer for solar fuel production is illustrated. In these hybrid systems a dye is used in a similar way as in the dye sensitized solar cells to absorb the energy from the sun, get excited and inject electrons to the CB of the semiconductor. The electrons are then transferred via the CB to a molecular catalyst that can catalyze the reduction reaction from for example CO_2 to CH_4 (10).

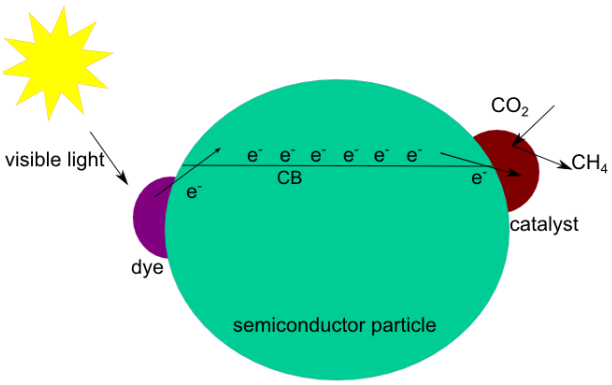

Figure 2.5. A schematic picture of a hybrid system approach for solar fuel production, inspired by dye-sensitized solar cells. The figure is adapted from reference (10).

There has been a lot of research in synthesizing efficient dyes, and there are many available dyes with fast electron injection to the CB of semiconductors, in this project an organic dye called D35 is used since it is well-studied and has shown good stability and performance in dye sensitized solar cells (21). The structure of D35 is shown in figure 2.6 below.

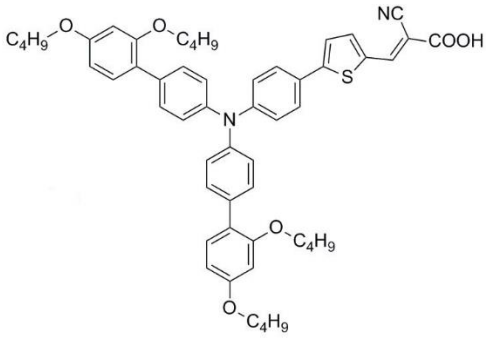

Figure 2.6. Structure of the organic dye D35 used in this project.

A main competitive reaction in these systems is when the electrons instead of being transferred to the catalyst recombines back to the dye. Since the goal is to transfer the electrons to an catalyst instead of collecting a current as in the dye sensitized solar cells, recombination to the dye will be the main competing pathway for the electrons (10). As could be seen in figure 2.3, an overlap with the oxidized stage of the molecule (necessary for the dye to inject electrons to the CB) corresponds to simultaneous overlap with the reduced state (29). Interfacial recombination is therefore a competing reaction to the electron transfer to the catalyst.

2.3.1. Protoporphyrin IX cobalt as model catalyst

In this project, protoporphyrin IX cobalt (CoPPIX) is used as the electron acceptor and model catalyst. It is used because it is well studied electrochemically, has a clear spectroscopic fingerprint and has shown some good catalytic activity for reduction of CO_2 (31) (32). Due to the carboxylic acid groups it can furthermore easily bind in to the semiconductors, since that group can work as an anchoring group (33). A figure of the structure of CoPPIX is shown in figure 2.7 below.

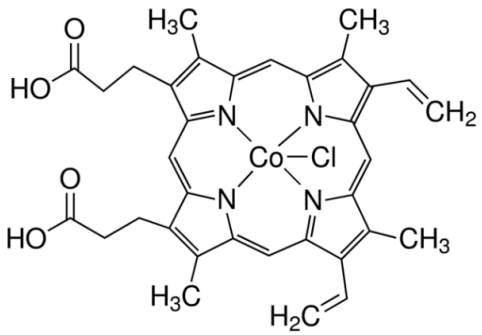

Figure2.7. Structure of protoporphyrin IX cobalt chloride, used as the model catalyst in this project.

CoPPIX is part of a group of molecules called porphyrins. All porphyrins have the same aromatic cycle, which most often has a metal ion in the center. The absorption spectrum of protoporphyrins has a strong Soret band around 400 nm and two weaker peaks in the Q-band between 500-600 nm (34). When Co-complexes are reduced their spectrum shifts, so in that way we can detect the reduction from for example Co^{III} to Co^{II} (35). When recording the spectrum while a reaction is ongoing, isobestic points can be observed. These are points in the spectrum where the molar absorptivity of two different compounds are the same. When having a reaction of the type $Co^{III} \rightarrow Co^{II} \rightarrow Co^{I}$, the isosbestic points can be used to monitor when the reaction reaches Co^{I}. This happens when the isosbestic points of the $Co^{III} \rightarrow Co^{II}$ reaction no longer can be observed. (36)

3. Method and materials

3.1. Chemicals

The following chemicals were used in this project:

- Protoporphyrin IX cobalt chloride (CoPPIX) (Sigma-Aldrich)
- Dimethyl sulfoxide (DMSO) (≥99.9% Sigma-Aldrich)
- Acetonitrile (MeCN) (≥99.5% Sigma-Aldrich)
- Ethanol (99,7%, Solveco)
- Methanol (MeOH) (99.8% Sigma-Aldrich)
- Isopropanol (≥99.5, Sigma-Aldrich)
- Titanium dioxide paste (18NR-T, Dyesol)
- Tin(IV) oxide colloidal dispersion (15% in water, Alfa Aesar)
- Tin(IV) oxide colloidal (SN15CG, Nyacol)
- Polyethylene glycol (PEG) (Mn=20 000, Sigma-Aldrich)
- Polyethylene glycol (PEG) (Mn=12 000, Alfa Aesar)
- Polyethylene oxide (PEO) (Mn=100 000, Alfa Aesar)
- Tetrabutylammonium hexafluorophosphate ($TBAPF_6$) (98.0%, Sigma-Aldrich)
- Dyenamo orange (D35) (Dyenamo)

3.2. Equipment

The following equipment was used during the project:

- Ultra 55 FEG SEM
- Two different Varian Cary 50 Bio UV-vis spectrophotometer
- Xenon-lamp
- Continuum Surelite Nd:YAG laser
- Surelite OPO
- QTH lamp
- 2 monochromators (Cornerstone 130, Oriel instruments)
- Photodiode detector (Hamamatsu S307)
- Filter box
- Oscilloscope (TDS 2022 – Tektronix)

3.3. Preparation of semiconductor-pastes

The TiO_2-paste was purchased and used directly without further modifications. Different methods were tested for synthesis of the SnO_2-nanoparticle paste. The first method was similar to what has been described in the literature (37), but with a lower temperature for the hydrothermal synthesis. First 2 ml of acetic acid was added to 30 ml of a colloidal dispersion of SnO_2 particles (15 wt% in H_2O). The solution immediately turned white and was left stirring at room temperature overnight and was then hydrothermally treated in 200 °C for 72 hours in a Parr instrument pressure vessel with a Teflon liner. The resulting solution was then ultrasonicated and 2.5 wt% of PEG and PEO was added and the solution was stirred overnight. More polymers were then added stepwise until the consistency was good (approximately another 5 wt% of each).

The SnO_2-paste used for the experiments was prepared from another dispersion of SnO_2 nanoparticles (Nyacol). 2 g of the colloidal was mixed with 0.15 g of polyethylenglycol (M_n= 20 000) and stirred for 1

hour. Then 0.4 ml of ethanol was added and the solution was stirred for 15 minutes and left over night. The paste was then stirred again for 15 min and 0.2 ml of water was added.

The mixed TiO_2/SnO_2 paste was prepared by adding five drops of isopropanol to 0.5 g of the TiO_2-paste. To this, 0.1 g of the SnO_2-paste was added and the mixture was ultrasonicated for 30 min, stirred for 5 min and then ultrasonicated for another 30 min and then used directly.

3.4. Preparation of thin films

Glass slides (conductive FTO-glass or non-conductive glass) was cut using a glass cutter with a diamond tip. After the glass slides were cut they were cleaned in a 3 % detergent solution of RBS in an ultrasonic bath for 15 min and then rinsed with water and ethanol and dried in air. The TiO_2 films were prepared from premade TiO_2 paste with the doctor blading method. In this method, two pieces of Scotch tape is put on the sides of the glass slide. A small amount of the paste is then put on one side of the glass and spread out evenly using a glass rod. The film thickness then becomes equal to the thickness of the tape (approximately 6 µm). The films were then allowed to dry at 125 °C and were then heated in several steps in an oven (150 °C 10 min, 200 °C 10 min, 250 °C 15 min, 300 °C 15 min, 400 °C 15 min) to 450 °C where they were sintered for 30 minutes.

The SnO_2 films were prepared by doctor blading the pastes on glass that then were heated in an oven in several steps (similar as for the TiO_2 films) to 350-450 °C where they were sintered for 30 min- 1 hour. The TiO_2/SnO_2 films were prepared by doctor blading the mixed paste on glass and heated in several steps in an oven to 450 °C where they were sintered for 30 min.

3.5. Sample preparation

To sensitize the films they were immersed in a 0.3 mM solution of CoPPIX in DMSO or a 0.3 mM solution of D35 in ethanol for different times to obtain the desired coverage, and then rinsed with ethanol and dried in air. To co-sensitize the films, they were first immersed in D35-solution for 50 minutes and then immersed in the CoPPIX-solution for 2 minutes.

For all the spectroscopic measurements the electrolyte used was 0.1 M $TBAPF_6$ in either DMSO or MeCN. The solutions were always purged with argon for at least 15 min before the experiments. For the transient absorption spectroscopy measurements, one droplet of the solution was put on a cover glass slide which was pressed onto the sample just before the measurements.

3.6. Scanning electron microscopy

Scanning electron microscopy (SEM) is used to characterize the morphology, chemical composition and crystalline structure of materials. Electrons are accelerated towards the sample and the interactions of the electrons with the sample is what produces the image. When using the Inlense detector the secondary electrons are detected and an image of the morphology of the films is obtained. When an EDX-detector is used, the elements of the sample can be determined from the X-ray emission of the sample. In this project SEM was used to determine the size of the nanoparticles, the morphology of the semiconductor films and the elements present in the films. (18)

3.7. Optical spectroscopy

The main techniques used to characterize the electron transfer in this project were different types of optical spectroscopy, including absorption spectroscopy and transient absorption spectroscopy. These techniques are described below.

3.7.1. Steady state UV-vis absorption spectroscopy

In this project UV-vis absorption spectroscopy was used to measure the absorption of the different films. It was also used examine if CoPPIX and D35 could bind in to the films.

In UV-vis absorption spectroscopy, the amount of light that a molecule absorbs at different wavelengths is measured. The absorbance (A) of the sample is linearly dependent on the product of the molar absorptivity (ε), the path length of the light (l) and the concentration of the sample in the solution (c), as described by the Lambert-Beer law (equation 5 below).

$$A = -log\frac{I_0}{I} = \varepsilon\, l\, C \tag{5}$$

3.7.2. Steady state photolysis experiments

Characterization of the electron transfer from the semiconductors to CoPPIX were done with photolysis experiments. In these experiments the semiconductors were band gap excited to promote VB-electrons to the CB with a Xenon lamp with a UV-filter (260 - 400 nm) together with a water filter to avoid heating of the filter, and the absorption spectrum was measured continuously. By looking at the changes in the spectrum, the spectroscopic signal of the CB-electrons can be studied and the reduced state of the acceptor can also be identified.

3.7.3. Nanosecond transient absorption spectroscopy

With nanosecond transient absorption spectroscopy, photoinduced changes in molecules can be measured. In this project it was used to measure the kinetics of the recombination from the semiconductors to D35.

In this technique, a fraction of the sample is first excited with a nanosecond light pulse of 10 ns (pump light). A continuous lamp (probe light) illuminates the sample at right angle to monitor the changes in absorption. A monochromator is situated before and after the sample at the path of the continuous lamp, and a detection system with a photodiode, filterbox and digital oscilloscope together with a computer is used to measure the transmitted light. A picture of the instrumental setup is shown in figure 3.1 below.

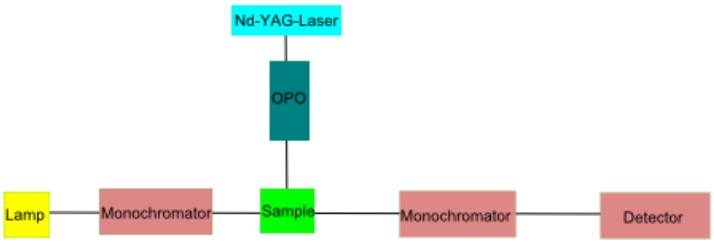

Figure 3.1. The instrumental setup for the nanosecond transient absorption spectroscopy measurements in this project.

The ground state of the molecule absorbs the pump light which produces a photoexcited state. After the photoexcitation, different physical and chemical processes occurs, some of these processes are too fast or too slow to be detectable using this technique while some of them can be measured. The transient absorbance ΔA(λ,t) is calculated by measuring the intensity of the transmitted light before

the excitation pulse and how it changes after; A(after pump)-A(before pump), see figure 3.2 below. Depending on the lifetime of the excited state for the sample, various processes can be detected for example the excited state or the charge separated state. (38) In this project it is the oxidized dye that is detected after the electrons have been injected to the CB, and ΔA(λ,t) is therefore A(oxidized state)-A(ground state) in our measurements.

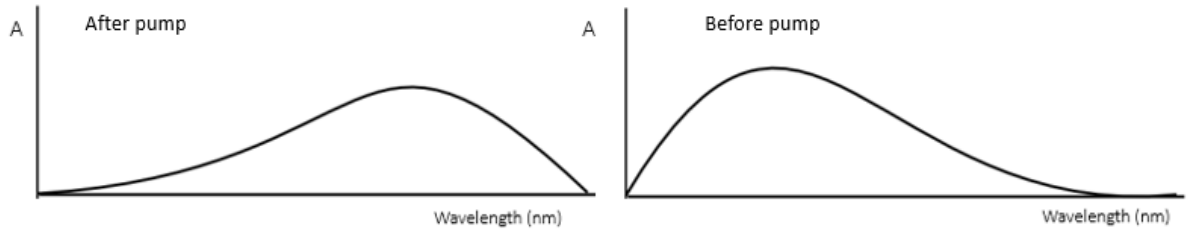

Figure 3.2. Schematic picture of a spectrum of a molecule after (left) and before (right) the laser pulse. ΔA is obtained by subtracting the spectrum of the excited state from the spectrum of the ground state.

ΔA in this project can essentially be described with equation 7 below:

$$\Delta A = \big(\varepsilon(oxidized\ state) - \varepsilon(ground\ state)\big) * l * c \qquad (7)$$

Where ε(oxidized state) and ε(ground state) is the extinction coefficient for the oxidized and the ground state respectively, l is the path length and c is the concentration of the sample. A negative signal in the graph of ΔA against the wavelength means that the extinction coefficient of the oxidized dye is lower than that of the ground state (ground state bleach). A positive signal means that the extinction coefficient of the oxidized dye is higher than that of the ground state (excited state absorption). (38)

A graph of ΔA against the wavelength gives information on how the spectrum is changed after the pump light has excited the sample. Plotting ΔA against the time at a fixed wavelength can give information about the kinetics of different processes, for example how fast the dye returns to the ground state. Figure 3.3 below shows a schematic illustration of ΔA(λ) and ΔA(t). (38)

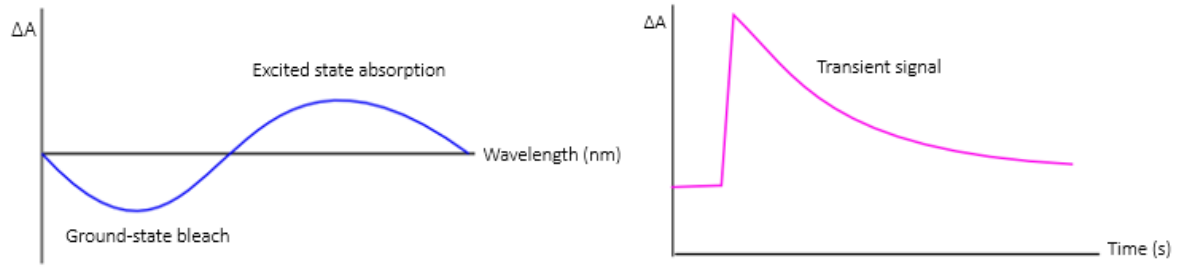

Figure 3.3. ΔA against the wavelength, obtained by subtracting the spectrum of the excited state from the original spectrum (left) and ΔA against the time for a transient decay at a fixed wavelength for the excited stage decay (right).

3.7.3.1. Fitting of curves

The curves with ΔA against time are fitted to exponential functions using the analysis tool in the program Origin Pro 2015. The best fits were obtained when a double exponential function was used, see equation 8 below. The rate constants were obtained from the reciprocal of the time constants.

$$I = I_0 + A1 * \exp\left(\frac{-x}{t1}\right) + A2 * \exp\left(\frac{-x}{t2}\right) \qquad (8)$$

3.8. Cyclic voltammetry

The redox potentials of the acceptor molecule was measured using cyclic voltammetry (CV). In CV, a system of three electrodes is used; a reference electrode that is used for calibration and kept constant during the measurement, a working electrode at which the redox reaction occurs and a counter electrode. The electrodes are immersed in an electrolyte and during the experiment the potential of the working electrode is varied and current flows between the working electrode and the counter electrode. The potential are varied first from the initial value (V_1) to a predetermined second value (V_2), and then back to the initial value, V_1 (39).

3.9. Spectroelectrochemistry

In spectroelectrochemical measurements both UV-vis absorption spectroscopy and electrochemical instruments are used at the same time. A system of three electrodes is used in a similar way as in CV. A potential is applied between the counter electrode and the reference electrode, and the current between the working electrode and the counter electrode is measured. At the same time, the absorption spectrum of the sample is measured, to see how the changes affects the spectrum and to identify the spectroscopic signal of the reduced/oxidized state of the molecule (40). In this project this technique was used to see how the spectrum of the reduced CoPPIX and oxidized D35 looked like and to characterize the electron transfer from the semiconductors to CoPPIX. An illustration of the instrumental setup is shown in figure 3.4.

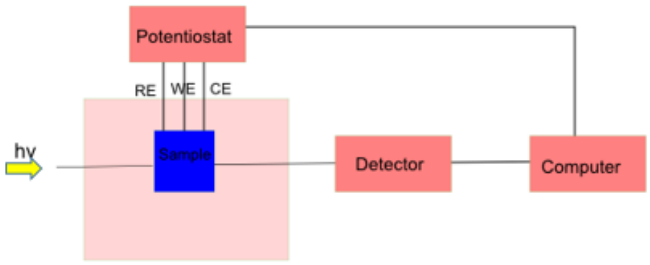

Figure 3.4. A schematic picture of a spectroelectrochemical measurements.

4. Results and Discussion

4.1. Characterization of the semiconductor films

After sintering in the oven, the TiO_2-films were transparent to blue and both D35 and CoPPIX adhered well to the surface. A SEM-image of a TiO_2-film is shown in figure 4.1, we can see that the particles are small (15-20 nm), which are suitable for use in dye sensitized solar cells and similar systems due to the high surface area and nanoporosity. This was a good and expected result since the paste used was a commercial available TiO_2-paste.

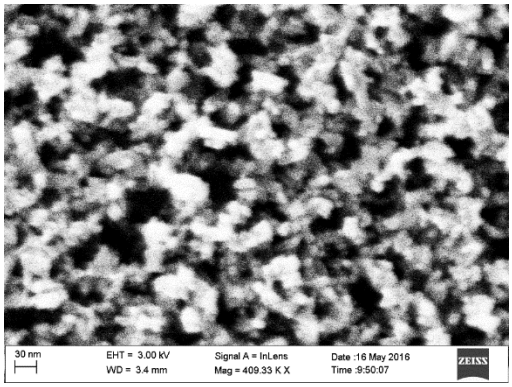

Figure 4.1. SEM image of a TiO_2-film made from the purchased paste, the particles are between 15-20 nm. The detector used is InLense and the high tension is 5.00 kV.

For the SnO_2-films there were some difficulties with too large particles. Different methods were tried for synthesizing the paste. The recipe involving hydrothermal treatment was tested two times, and from the SEM picture in figure 4.2a) it is clear that the process is highly uncontrolled and that very large particles are formed. These particles have too low surface area, and the films were too opaque to be useful in this project. This result suggest that hydrothermal synthesis at 200 °C is an uncontrolled process that not is good for obtaining nanoparticles with a small size and narrow size distribution. It is difficult to know why the synthesis did not succeed, it could be because of the lower temperature used compared to the reference. The hydrothermal synthesis of the paste was supposed to be at 240 °C according to the reference, but due to lack of a reactor that could withstand so high temperature the synthesis was instead performed at 200 °C. However why a lower temperature would give larger particles is not clear, since according to the literature of hydrothermal synthesis the particles should grow more as the temperature gets higher. The expected result would then be that the particles got smaller. One possible reason could be that at 200 °C, the crystallization process does not occur but instead we only get large agglomerates from the original particles.

The alternative method for preparing SnO_2-paste from another colloidal dispersion of SnO_2-particles yielded a better size of the particles (~10 nm), see figure 4.2b) below. This paste however was too thick to prepare homogenous films. The films prepared from this paste were furthermore falling of the glass, especially when immersed in the D35- and CoPPIX-solutions. The reason for the uneven films and the thick consistency of the paste could be that the starting material had gelled, it is likely that this change in consistency also affected the consistency of the final paste.

Improvement of the method to prepare a SnO_2-paste is needed in order to get films that adhere better to the surface. Despite their low adhesiveness, those films were used for the measurements due to their transparency and nanoparticle characteristics.

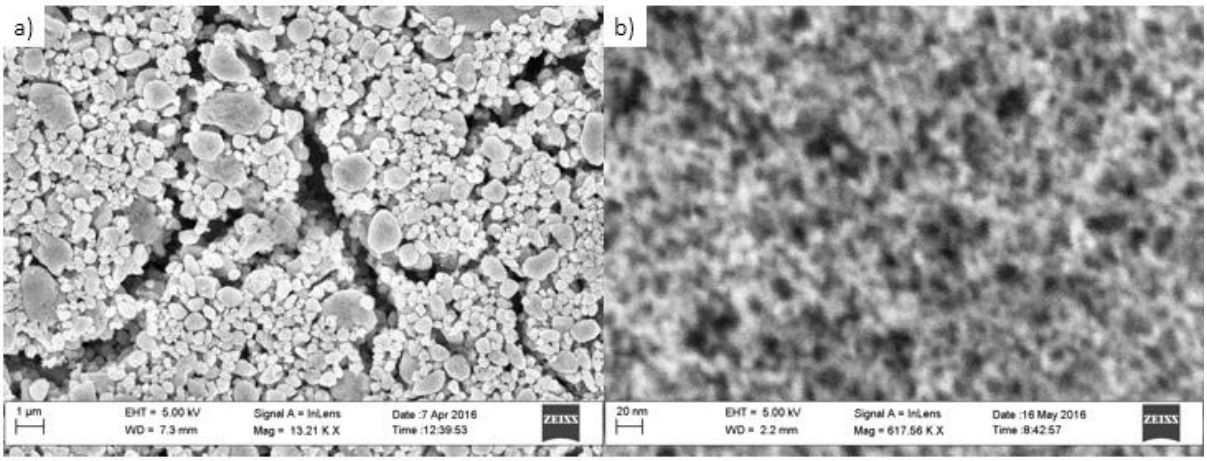

Figure 4.2. a) SEM image of a SnO_2-film made from the hydrothermal method, these particles are too large (100 – 1000 nm) to be useful in this project. The detector used is InLense and the high tension is 5.00 kV. b) SEM image of a SnO_2-film made from the alternative method, the particles are around 10 nm. The detector used is InLense and the high tension is 5.00 kV

In figure 4.3, a SEM-image of a mixed TiO_2/SnO_2-film is shown. After sintering in the oven, these films were transparent to white. The particles seems homogenously mixed and we cannot observe any large agglomerates containing only one type of particle. The particles are a bit larger than in the other films (~20-30 nm) but the films are still nanoporous.

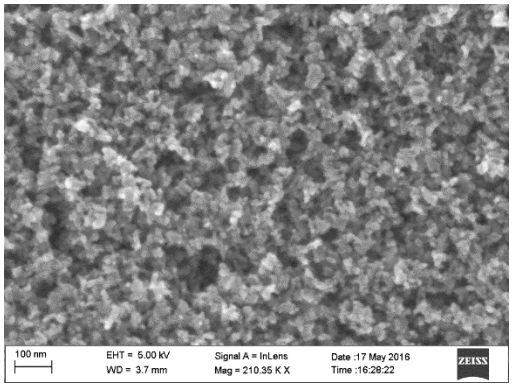

Figure 4.3. SEM image of a TiO_2/SnO_2-film made from the mixed paste. The particles look very well mixed and the size of them are between 20-30 nm. The detector used is InLense and the high tension is 3.00 kV.

To make sure that both TiO_2 and SnO_2 were present in the film, EDX-analysis was performed. Three different spots on the film were chosen and all had similar composition. The EDX-analysis demonstrated that both Ti and Sn are present in the film and that there is about ten times more Ti than Sn, which is likely since more TiO_2-paste was added to the mixture. The composition from the EDX analysis is presented in table 4.1 below and the full EDX-analysis can be found in appendix A. In order to have a similar proportion of Ti and Sn, both pastes should be either water or organic solvent based. Then probably more even distribution of the pastes could have been used without destabilizing the particles.

Table 4.1. The composition of the mixed film obtained from the EDX-analysis.

Spectrum	**O (%)**	**Ti (%)**	**Sn (%)**
Spectrum 1	70.48	27.00	2.52
Spectrum 2	71.07	26.55	2.38
Spectrum 3	69.71	27.67	2.62

4.2. Characterization of D35 and Protoporphyrin IX cobalt

The absorption spectrum of the dye D35 and the acceptor CoPPIX on a TiO_2 film is shown in figure 4.4a) and the absorption spectrum of a co-sensitized TiO_2-film is shown in figure 4.4b). The dye D35 has a broad absorption peak between 400 – 550 nm and can therefore absorb a lot of that light, CoPPIX has a characteristic Soret band at around 425 nm and two weaker peaks corresponding to the Q-band between 500-600 nm. This figure is used to decide where the sample should be pumped with the laser in the TAS experiments, the chosen wavelength is 532 nm to selectively excite the dye.

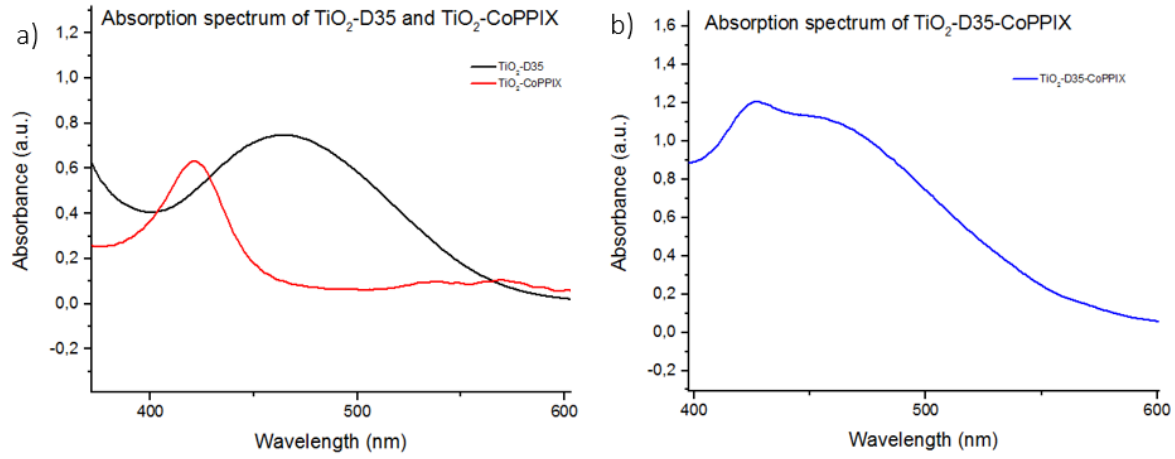

Figure 4.4. a) Absorption spectrum of D35 on a TiO_2-film (black line) and absorption spectrum of CoPPIX on a TiO_2-film (red line). b) Absorption spectrum of D35 and CoPPIX on a TiO_2-film.

The differential spectrum of D35 and CoPPIX on TiO_2 after oxidation and reduction respectively is shown in figure 4.5 below, with the original spectrums used as the baseline. From this figure it is possible to identify a wavelength where only the oxidized D35 absorbs, and that therefore can be selected as probe wavelength in the TAS measurements. The selected probe wavelength is 700 nm to selectively detect the recombination of electrons to D35.

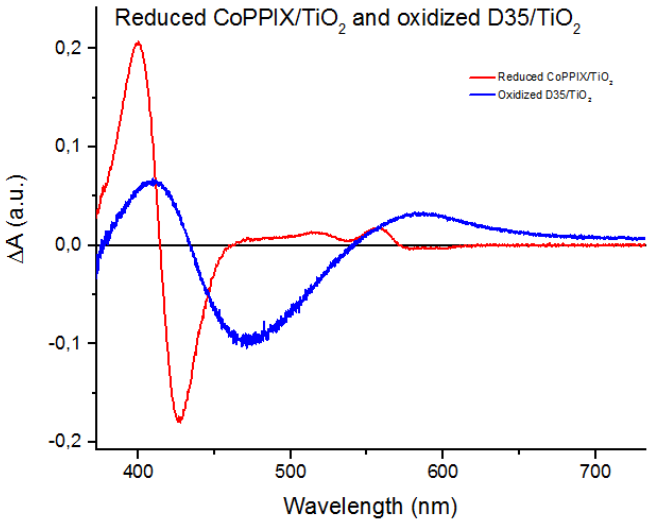

Figure 4.5. Differential absorption spectrum of oxidized TiO_2- D35 obtained with spectroelectrochemistry in 0.1 M $LiClO_4$ (performed by Valeria Saavedra) and reduced CoPPIX obtained from spectroelectrochemistry measurement in 0.1 M $TBAPF_6$.

The reduction potential of CoPPIX was measured from a CV-experiment performed in fluid solution, see figure 4.6.

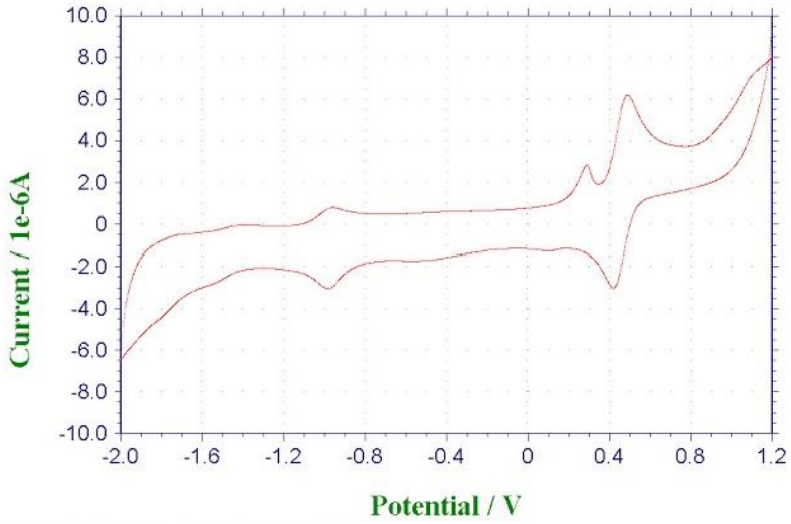

Figure 4.6. CV of 0.3 mM CoPPIX in 0.1 M $TBAPF_6$ in DMSO with ferrocene as the reference, this experiment is an unpublished result performed by Valeria Saavedra. The WE is glassy carbon, the CE is Pt and the RE is SCE. The large peak at 0.5 V is from ferrocene.

There is a weak peak at 0.15 V vs SCE which can be assigned to the reduction of Co^{III}/Co^{II}, this peak is about -0.3 V vs ferrocene, corresponding to about 0.5 V vs NHE. CoPPIX is therefore likely to be a suitable electron acceptor from SnO_2. The CB-potential of TiO_2 and SnO_2 is more negative than the reduction potential of CoPPIX and therefore we could not identify a peak corresponding to reduction of CoPPIX when performing CV-experiment with CoPPIX attached to the semiconductor films. The reduction potential for CoPPIX on the films is therefore assumed to be similar to the value measured in solution and be below the CB of SnO_2. An energy diagram illustrating the reduction potential of CoPPIX in comparison to TiO_2 and SnO_2 is illustrated in figure 4.7 below. According to the literature, the half way potential of D35 is much more positive than the acceptor (around 1.3 V vs NHE) (41), therefore electron transfer from the dye to the acceptor is unlikely to occur. However it is possible that electrons can be transferred from the acceptor to the dye.

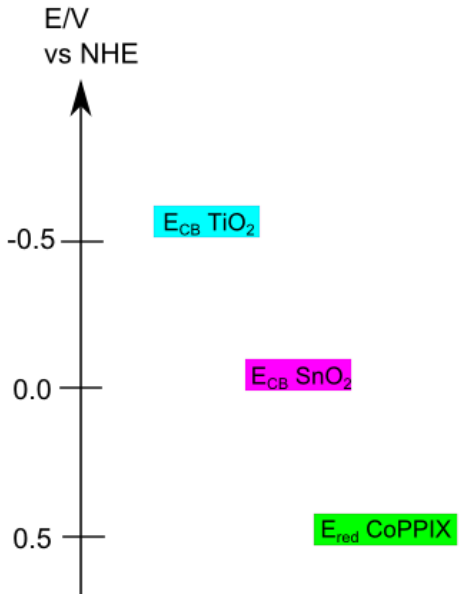

Figure 4.7. The CB-potentials of TiO_2 and SnO_2 compared to the reduction potential of CoPPIX measured from CV in solution.

4.3. Conduction band mediated reduction of Protoporphyrin IX cobalt

To investigate the possibility of using these dye-semiconductor-acceptor assemblies for photocatalysis, the CB mediated electron transfer from the semiconductors to CoPPIX were characterized.

As can be seen in figure 4.8, electrons are accumulated in the CB of TiO_2, both when a negative potential is applied and when the film is illuminated with UV light. The CB electrons are seen in the spectrum as a broad absorption above 500 nm that increases as more light has illuminated the sample or when a more negative potential has been applied. These results demonstrates that it is possible to accumulate a lot of electrons in the CB. This also suggests that, when there is a driving force for the electron transfer, the CB-electrons can be transferred to acceptor molecules on the surface of the semiconductor.

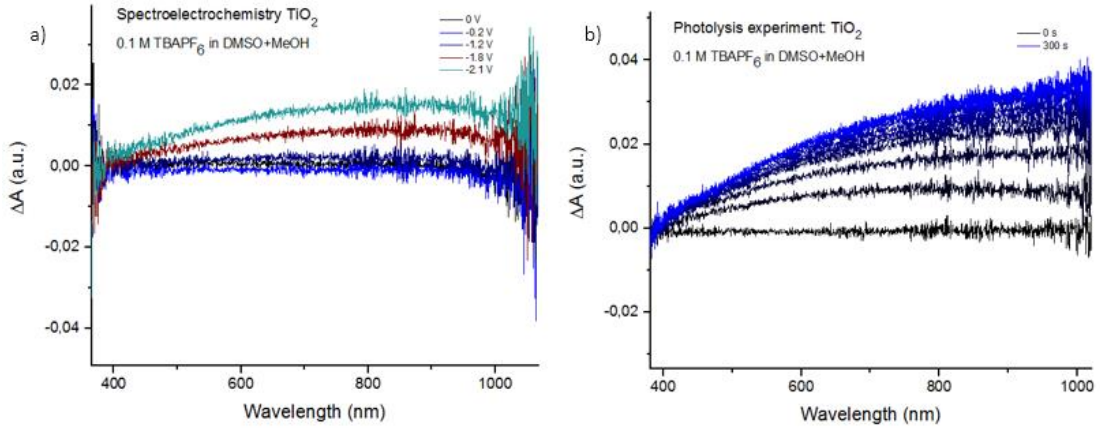

Figure 4.8. a) Differential spectrum of a TiO_2-film in 0.1 M $TBAPF_6$ in DMSO with a few drops of MeOH while a multistep potential is applied. The WE is FTO-glass with a thin TiO_2-film, glassy carbon is used as CE and Ag/Ag^+ as the RE. b) Differential spectrum of a TiO_2-film in 0.1 M $TBAPF_6$ in DMSO with a few drops of MeOH while the films it is illuminated with a Xenon-lamp with a UV-filter. The spectrum is recorded every 30 seconds.

4.3.1. Reduction of Protoporphyrin IX cobalt on TiO_2

The differential spectrum from a spectroelectrochemical measurement on TiO_2-CoPPIX is shown in figure 4.9. When a negative potential is applied the spectrum starts to change, corresponding to the reduction of CoPPIX since a driving force is applied for the electron transfer. Since a negative potential is applied, this reduction does not necessarily has to be CB mediated, there are other mechanisms for electron transfer directly from the conductive glass as well (42).

The peaks at 425 nm and 575 nm decreases as more negative potentials are applied and new peaks at 400 nm and 555 nm appears. This corresponds to the reduction of the sample. It seems like we have one reduction, Co^{III}/Co^{II}, since the isosbestic points at 415 nm and 455 nm are constant throughout the experiment. The shifts in the Soret band corresponds well to the reported shifts in the spectrum from the reduction Co^{III}/Co^{II} in another Co-porphyrin, Co(TCPP)Cl[2] (35).

[2] TCPP= meso-5,10,15,20-tetrakis(4-carboxyphenyl)porphyrin

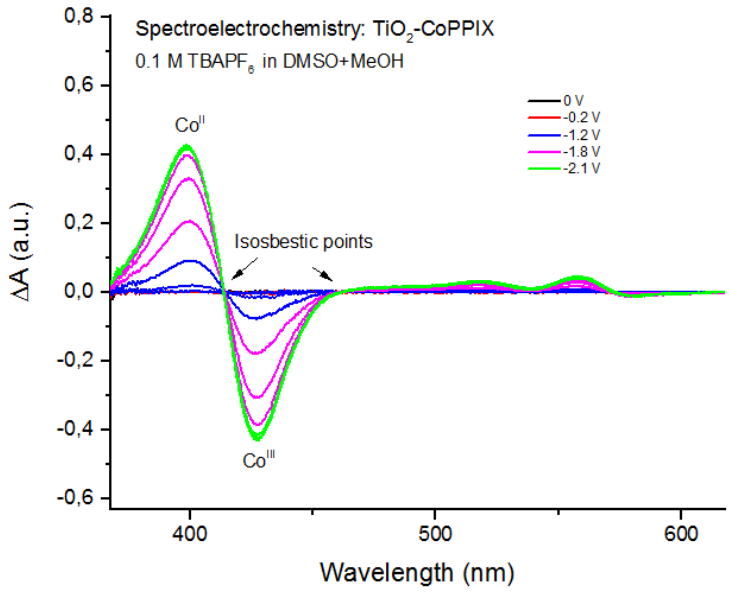

Figure 4.9. Differential spectrum of a TiO_2-CoPPIX-film in 0.1 M$TBAPF_6$ in DMSO with a few drops of MeOH as sacrificial donor (argon purged for 15 min) while a multistep potential of -0.2 V -1.2 V -1.8 V and -2.1 V is being applied (90 s/step), TiO_2-CoPPIX on conductive FTO-glass is the WE, the RE is Ag/Ag+ and the CE is glassy carbon. The spectrum is recorded every 30 seconds.

A photolysis experiment was also performed on a TiO_2-CoPPIX film, the differential spectrum from this experiment is shown in figure 4.10. This spectrum is taken while the sample is illuminated with UV-light to band gap excite the TiO_2. The changes in the spectrum are similar to the changes in the spectroelectrochemistry experiment and hence CoPPIX get reduced.

The peak corresponding to Co^{III} at 425 nm is steadily decreasing during the experiment, so the amount of Co^{III}PPIX is decreasing throughout the experiment. The peak corresponding to Co^{II} at 400 nm is first increasing, but after about 120 seconds it starts to decrease again. This could be an indication that also the third oxidation state, Co^{I} is formed. A clear isosbestic point is visible at 415 nm for the first 120 seconds, probably where the extinction coefficients for Co^{III} and Co^{II} are the same. The disappearance of this point corresponds well to the decrease of the peak for Co^{II} at 400 nm and also to the appearance of a new peak at 480 nm. This indicates that the new peak at 480 nm could be from Co^{I}, this peak is not found in the literature so the increase in absorbance at 480 nm could also be the CB-electrons that becomes more visible. There is however an overall low absorbance from the CB-electrons in this spectrum, so this new peak is most probably from the Q-band of the Co^{I} state. According to the literature, Co^{I} has another peak at 375 nm in another Co-porphyrin (35). That peak is not visible in this spectrum so it is not clear if Co^{I} is created, but most probably it is since the isosbestic point is disappearing.

The other isosbestic point at 455 nm is visible throughout the entire experiment, at this point the extinction coefficient for all oxidation states of Co is probably be the same. The immediate overall increase in absorption after 500 nm is probably due to the increased amount of electrons in the CB. The changes in the spectrum occurs quickly, so the kinetics for the reduction of CoPPIX from illumination with UV-light is fast and the electron transfer to CoPPIX seems to be very efficient.

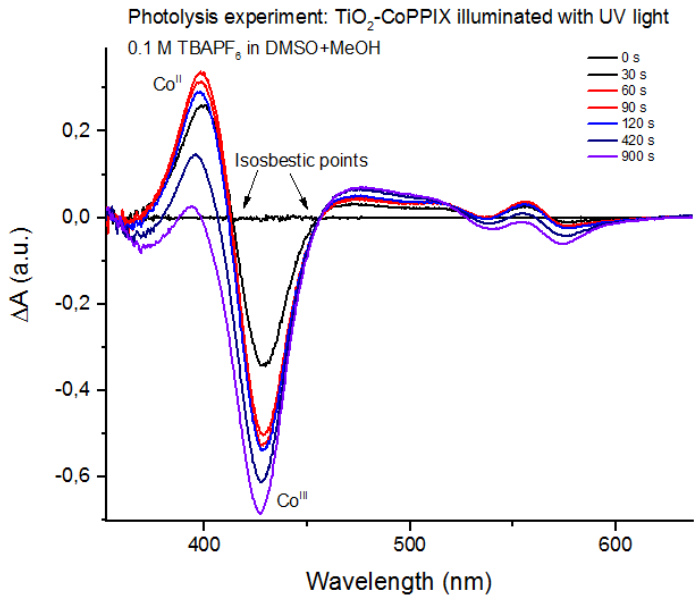

Figure 4.10. Differential spectrum of a TiO_2-CoPPIX-film in 0.1 M$TBAPF_6$ in DMSO with a few drops of MeOH as sacrificial donor (argon purged for 15 min) while it is illuminated with a Xenon-lamp with a UV-filter and a water-filter to avoid heating of the filter. The spectrum is recorded every 30 seconds.

When a solution of CoPPIX was illuminated with UV-light the same changes were not observed in the spectrum and when a film with CoPPIX on TiO_2 was put in the same electrolyte without being illuminated with UV-light, there was a very little autoreduction, see figures in appendix B. Since CoPPIX in solution does not get reduced from illumination of UV-light or get autoreduced while being attached to a TiO_2-film, the observed changes in the spectrum in figure 4.10 are attributed to CB mediated electron transfer to CoPPIX from TiO_2. If we look at the absorption after 500 nm in figure 4.10 we can also see an overall increase, which is from the CB-electrons that get transferred to the acceptor. The time-scale for this processes also corresponds well to the time-scale that electrons are accumulated in the CB (see figure 4.8), which is another indication that this process is CB-mediated. The reason for the differences between the spectroelectrochemistry and the photolysis experiments could be that there are different mechanisms for the reduction in the different experiments. In the photolysis experiment we are sure that it is the through the CB while for the spectroelectrochemical experiment it could be from another mechanism.

To investigate the effect of the solvent, a photolysis experiment was performed with the same electrolyte but in MeCN. As can be seen in figure 4.11, this resulted in a similar trend but the kinetics for the electron transfer seems to be much slower in this solvent.

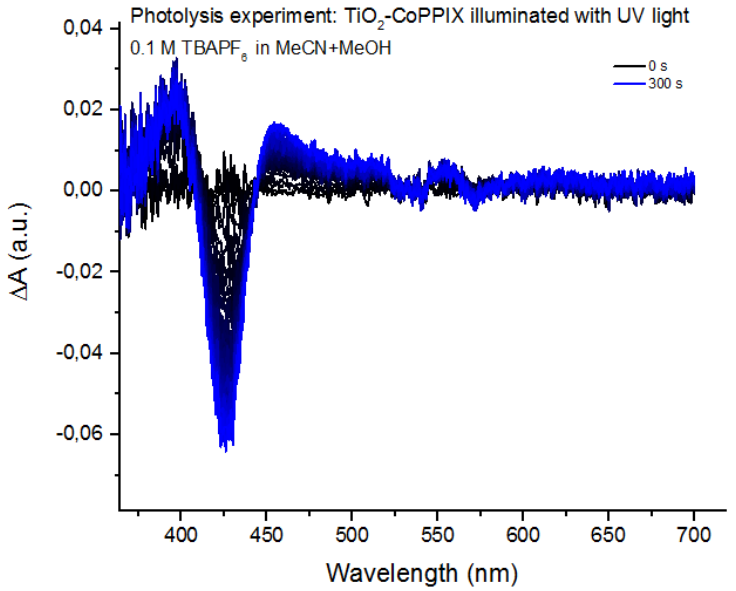

Figure 4.11. Differential spectrum of a TiO_2-CoPPIX-film in 0.1 M $TBAPF_6$ in MeCN with a few drops of MeOH as sacrificial donor (argon purged for 15 min) while it is illuminated with a Xenon-lamp with a UV-filter and a water-filter to avoid heating of the filter. The spectrum is recorded every 30 seconds.

4.3.2. Reduction of Protoporphyrin IX cobalt on SnO_2

To study the electron transfer from SnO_2 to CoPPIX, spectroelectrochemical and photolysis experiments were also performed on SnO_2-CoPPIX films. Since DMSO was the best solvent for this experiment on TiO_2, it was the solvent of choice for these experiments. The SnO_2-films were as previously mentioned more uneven and had lower coverage of CoPPIX than the TiO_2-films, so these spectrums has a lower absorption. Still we can see that CoPPIX gets reduced since the peaks are shifting when a negative potential is applied. The differential spectrum from the spectroelectrochemistry experiment is shown in figure 4.12 below.

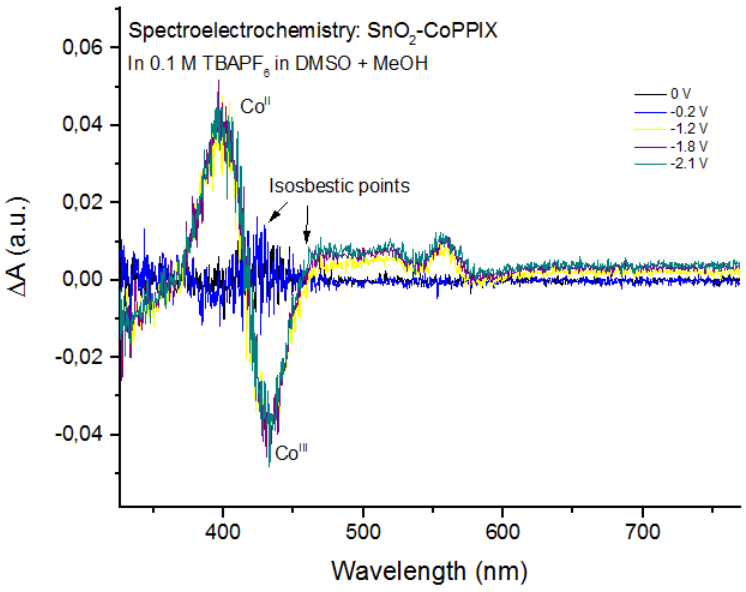

Figure 4.12. Differential spectrum of a SnO_2-CoPPIX-film in 0.1 MTBAPF$_6$ in DMSO with a few drops of MeOH as sacrificial donor (argon purged for 15 min) while a multistep potential of -0.2 V -1.2 V -1.8 V and -2.1 V is being applied (90 s/step), SnO_2- CoPPIX on conductive FTO-glass is the WE, the RE is Ag/Ag+ and the CE is glassy carbon. The spectrum is recorded every 30 seconds.

The changes in the spectrum corresponds to the reduction of CoPPIX. The reduction seem to happen from a less negative potential on these films compared to the TiO_2-films. All the observed changes occurred by applying a potential of -1.2 V (vs Ag/Ag^+) while for the TiO_2-CoPPIX experiments the spectrum changed steadily until a potential of -1.8 V (vs Ag/Ag^+) had been applied. This could indicate that there is another mechanism for the reduction for the SnO_2-films than for the TiO_2-films. The CB-electrons are also seen much faster in this spectrum, this could be because the coverage of CoPPIX was less on these films making the CB-electrons more visible.

The differential spectrum from the photolysis experiment with SnO_2-CoPPIX is shown in figure 4.13 below. The trend is similar as in the spectroelectrochemistry experiment. Also here we can see a broad absorption above 500 nm quickly, most probably from the CB-electrons.

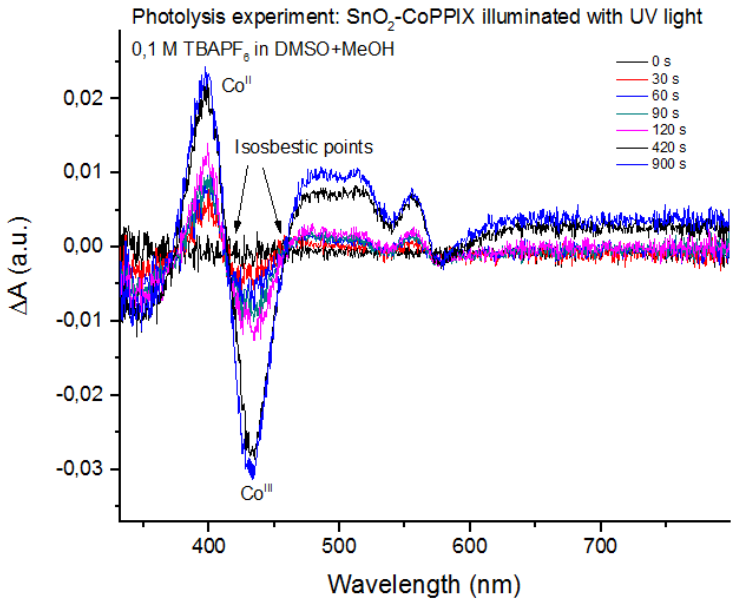

Figure 4.13. Differential spectrum of a SnO_2-CoPPIX-film in 0.1 MTBAPF$_6$ in DMSO with a few drops of MeOH as sacrificial donor (argon purged for 15 min) while it is illuminated with a Xenon-lamp with a UV-filter and a water-filter to avoid heating of the filter. The spectrum is recorded every 30 seconds.

Due to the low absorbance and noisy signal in these spectrums it is more difficult to see the isosbestic points or deduce when they deduce, but it looks like both the isosbestic at 415 and 455 nm are present throughout this experiment. This is an indication that only the reduction from Co^{III}/Co^{II} is occurring. The kinetics for the CB mediated reduction on SnO_2 seems to be a bit slower than on TiO_2, it seems like we only have one reduction on SnO_2 while there are two reductions on TiO_2 in the same experiment. The slower kinetics could be due to the lower driving force for the electron transfer between SnO_2-CoPPIX than between TiO_2- CoPPIX (see figure 4.7).

When the spectrum of a SnO_2-CoPPIX film was recorded without illuminating it with UV-light or applying a potential the same changes were not seen, see appendix B. So the reduction, even if it is not as clear as for TiO_2, is most likely due to conduction band mediated electron transfer.

4.4. Interfacial recombination kinetics

The effect of different solvents and conditions for the recombination kinetics were studied using TAS. The different solvents used were DMSO and MeCN with and without MeOH as sacrificial donor. All the measurements were done in triplicates and the curves were normalized, when one measurement differed from the others it was excluded.

4.4.1. Recombination on TiO_2

The normalized TAS-spectrum with the corresponding double exponential fits for the different samples in DMSO are shown in figure 4.14 below.

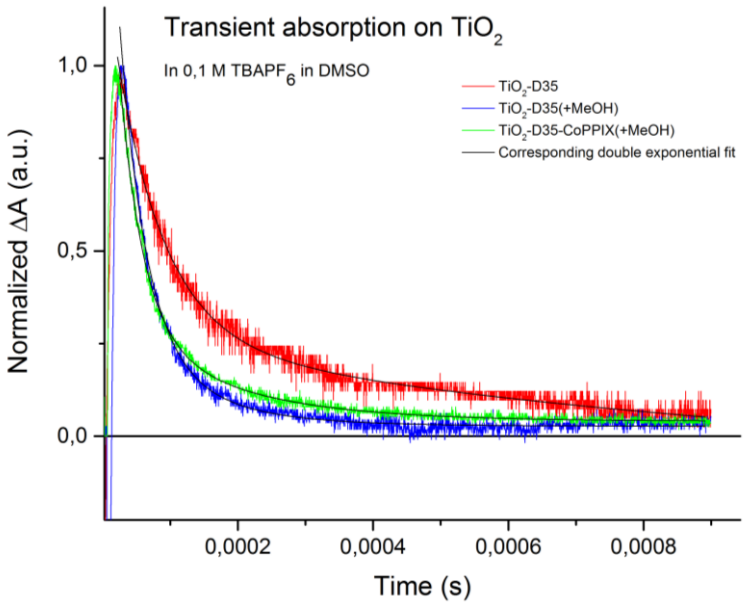

Figure 4.14. Normalized TAS-spectrum for the TiO_2-samples in DMSO recorded with a photodiode detector. The absorption spectrum for the films was measured before the TAS experiments and was kept at 0.3 (+/- 0.1) at the pump wavelength 532 nm for all samples. The power from the pump at the sample was 4 mW for the TiO_2-D35 samples and 1.2 mW for the co-sensitized films.

In DMSO, the incorporation of an acceptor does not significantly affect the recombination rate, but it becomes consistently slightly faster. Addition of MeOH also results in an increase of the recombination rate, this was unexpected since MeOH was added as a hole scavenger.

The normalized TAS-spectrum with the corresponding double exponential fits for the different samples in MeCN is shown in figure 4.15.

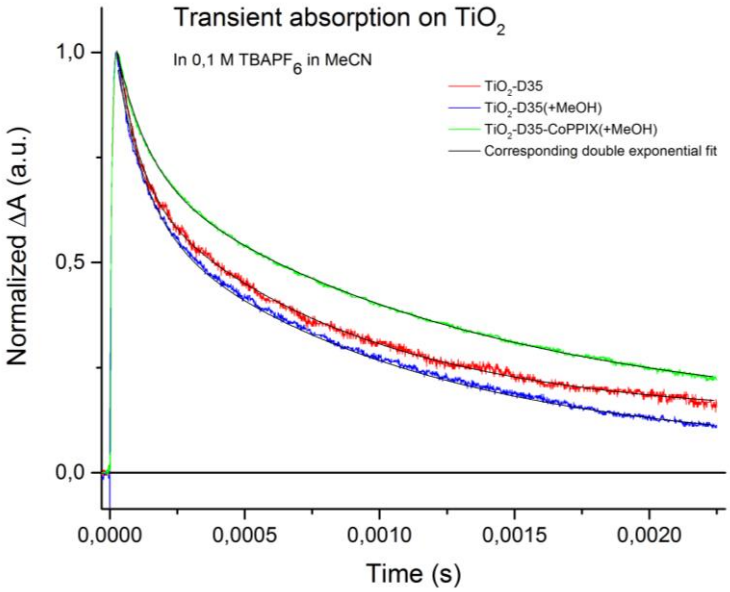

Figure 4.15. Normalized TAS-spectrum for the TiO_2-samples in MeCN recorded with a photodiode detector. The absorption spectrum for the films was measured before the TAS experiments and was kept at 0.3 (+/- 0.1) at the pump wavelength 532 nm for all samples. The power from the pump at the sample was 4 mW for the TiO_2-D35 samples and 1.2 mW for the co-sensitized films.

The lifetime of the charge separated state is much longer in MeCN than in DMSO. The ΔA does not reach zero after 250 μs for the samples in MeCN while for DMSO it is almost at zero for all the samples already after 100 μs. In MeCN, the incorporation of the acceptor makes the curves flatten out and the recombination slower. The calculated rate constants are presented in table 4.2.

Table 4.2. The calculated rate constants and amplitudes for the double exponential fits for the TiO_2-D35 and TiO_2-CoPPIX samples in different solutions. The values are calculated as mean values between the different double exponential fits for the samples in the same solution.

Sample	**k1 (10^{-4} s^{-1})**	**A1 (%)**	**k2 (10^{-4} s^{-1})**	**A2 (%)**
DMSO				
TiO_2-D35	1.3	79	0.2	21
TiO_2-D35 (+MeOH)	1.6	83	0.9	17
TiO2-D35-CoPPIX (+MeOH)	3.2	88	0.5	22
MeCN				
TiO_2-D35	1.0	57	0.1	43
TiO_2-D35 (+MeOH)	1.1	50	0.1	50
TiO_2-D35-CoPPIX (+MeOH)	0.8	30	0.07	70

The rate constants are smaller in MeCN than in DMSO, the fast component of the decay also has a greater contribution to the overall recombination in DMSO. These results suggest that the charge separated state has a longer lifetime in MeCN than in DMSO.

The fast component, k1, is not significantly affected by the addition of MeOH in neither of the solvents. But in DMSO, the slow component k2 increases from around $0.2*10^4$ s^{-1} to $0.9*10^4$ when MeOH is added, which is a significant increase. MeOH is a hole scavenger, but how this makes the recombination faster is not clear. Since MeOH is a polar solvent it could maybe interact with the surface in some way that helps the electron transfer.

The rate constants become higher in DMSO+MeOH when incorporating the acceptor. This suggests that the electrons do not reach the acceptor, or that the electrons that reaches the acceptor can be transferred directly to D35, making the recombination rate faster. In MeCN+MeOH, there is an opposite trend, the recombination rate decreases for the co-sensitized films, there is a small decrease in both k1 and k2. The amplitudes also changes a lot for this samples, making the contribution from the slower component larger. This could indicate that the electrons have been transferred to the acceptor from the CB. Since the contribution from the fast component decreases, it is probably the electrons corresponding to the fast component that are transferred to the acceptor instead of back to the dye.

4.4.2. Recombination on SnO_2

The normalized TAS-spectrum for the measurements on the SnO_2-D35 films in DMSO are shown in figure 4.16. Compared to the TiO_2-films, the SnO_2-films had lower dye coverage due to the reasons mentioned earlier.

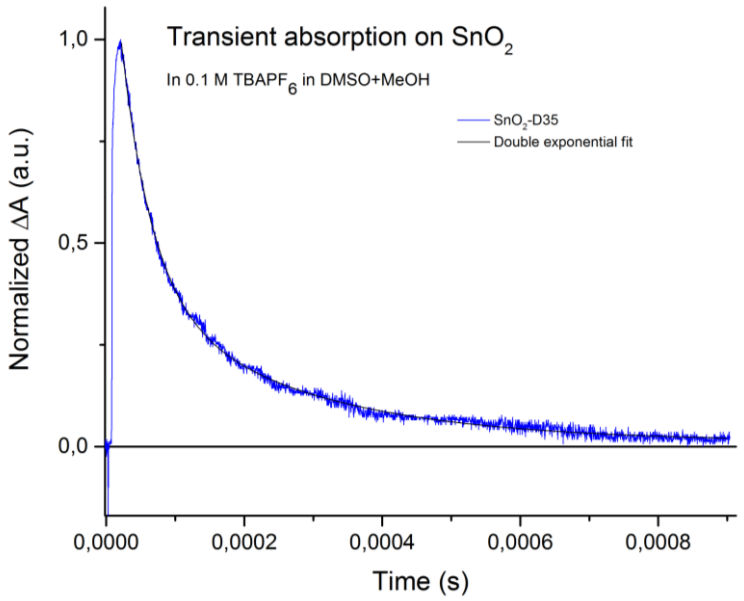

Figure 4.16. Normalized TAS-spectrum for the SnO_2-samples in DMSO recorded with a photodiode detector. The absorption spectrum for the films was measured before the TAS experiments and was kept at 0.2 (+/- 0,1) at the pump wavelength 532 nm for all samples. The power from the pump at the sample was 0.7 mW.

In figure 4.17 below is the normalized TAS-spectrum for the measurements in MeCN+MeOH.

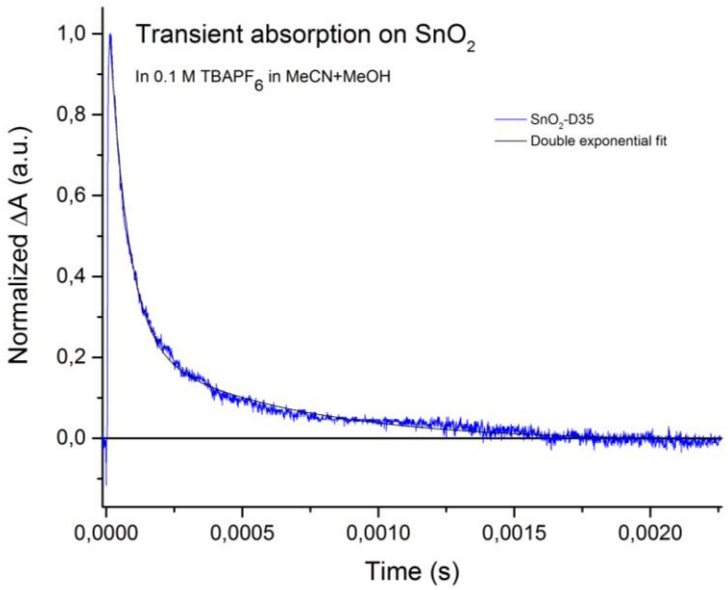

Figure 4.17. Normalized TAS-spectrum for the SnO_2-samples in MeCN recorded with a photodiode detector. The absorption spectrum for the films was measured before the TAS experiments and was kept at 0.2 (+/- 0,1) at the pump wavelength 532 nm for all samples. The power from the pump at the sample was 0.7 mW.

These experiments follows the same trend as earlier, the recombination is faster in DMSO than in MeCN. The reason for the faster recombination in DMSO for all samples could be that DMSO interacts with the surface in some way that helps the electron transfer. It is known that DMSO can coordinate to different metal complexes (43), but since D35 is an organic dye it is difficult to understand how this would have an effect for the recombination. The effect of the solvent follows the same trend as for the photolysis experiment. The kinetics for photoreduction of CoPPIX in DMSO is very fast while for MeCN it takes longer time for the electron transfer to occur. In this case it is likely that DMSO coordinates to cobalt in the complex and that it helps the electron transfer. The calculated rate constants for the recombination on SnO_2 are presented in table 4.3 below.

Table 4.3. Mean values of the calculated rate constants and amplitudes for the double exponential fits for the SnO_2-D35 sample. The values are calculated as mean values between the different double exponential fits for the samples in the same solution.

Sample	**k1 (10^{-4} s^{-1})**	**A1 (%)**	**k2 (10^{-4} s^{-1})**	**A2 (%)**
DMSO+MeOH				
SnO_2-D35	2.1	71	0.4	29
MeCN+MeOH				
SnO_2-D35	1.6	77	0.2	23

The recombination is faster for SnO_2-D35 than for corresponding experiment with TiO_2-D35, both rate constants are larger in both solvents for the SnO_2-samples than for corresponding TiO_2-samples. There is also a greater contribution from the faster component for these samples. These results indicate that a mixed system with dye-TiO_2/SnO_2-acceptor should be more efficient than corresponding system with only one semiconductor. This because in these systems it is desirable to have slow electron transfer from TiO_2 to the dye and fast electron transfer from SnO_2 to the acceptor.

No additional experiments with SnO_2 films were performed, it was not possible to co-sensitize the films because all D35 desorbed when trying to attach the CoPPIX.

4.4.3. Recombination on TiO_2/SnO_2

Since all results from the previous measurements suggests that MeCN is the best solvent for minimizing the recombination, it is the solvent of choice for the experiments with the TiO_2/SnO_2-films. The normalized TAS-spectrum for the measurements with the TiO_2/SnO_2-films is shown in figure 4.18.

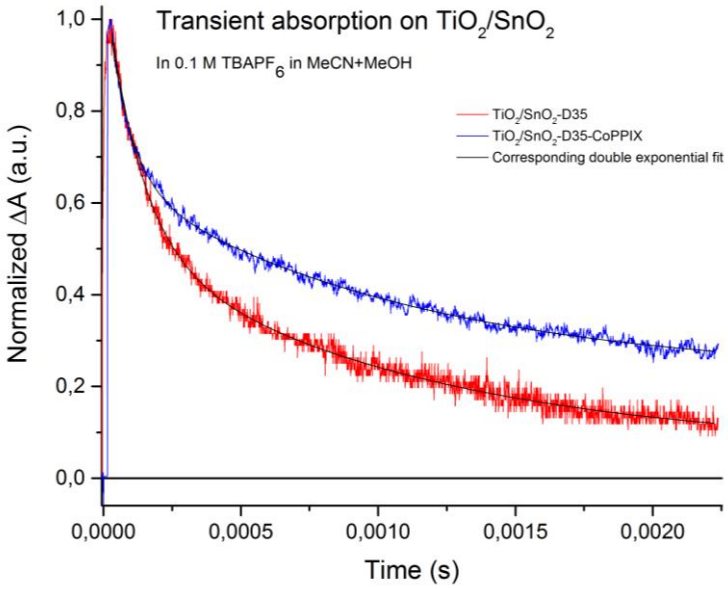

Figure 4.18. Normalized TAS-spectrum for the TiO_2/SnO_2-samples in MeCN recorded with a photodiode detector. The absorption spectrum for the films was measured before the TAS experiments and was kept at 0.3 (+/- 0.1) at the pump wavelength 532 nm for all samples. The power from the pump at the TiO_2/SnO_2-D35 samples was 1.3 mW and the power at the TiO_2/SnO_2-D35-CoPPIX was 1.0 mW.

Here we see a clear difference between the co-sensitized films and the films with only D35. The fast decay in the beginning is similar for both systems, but then the co-sensitized films seem to flatten out, indicating that some electrons are transferred to CoPPIX instead of to D35. The calculated rate constants for the recombination on TiO_2/SnO_2 are presented in table 4.3 below.

Table 4.4. Mean values of the calculated rate constants and A-values for the double exponential fits for the SnO_2-D35 sample. The values for the double-sensitized films are obtained from the double exponential fit for an experiment for 500 µs. The values are calculated as mean values between the different double exponential fits for the samples in the same solution.

Sample	**k1 (10^{-4} s^{-1})**	**A1(%)**	**k2 (10^{-4} s^{-1})**	**A2(%)**
MeCN+MeOH				
TiO_2/SnO_2-D35	0.7	67	0.09	33
TiO_2/SnO_2-D35-CoPPIX	0.9	50	0.05	50

The recombination rate for TiO_2/SnO_2-D35 is similar as for TiO_2-D35 and slower than for SnO_2-D35. The rate constants are smaller for the TiO_2/SnO_2-samples than for the TiO_2-samples, but the contribution from the fast component is greater for the TiO_2/SnO_2-samples making the overall recombination similar.

The rate constants are not significantly affected by the incorporation of the acceptor, the fast component becomes a bit larger while the slow component becomes smaller. There is however a difference in the amplitudes, the slower component has a larger contribution than the faster component for the co-sensitized film. This follows the same trend as for the co-sensitized TiO_2-film,

and probably also here the electrons that usually recombines fast are the ones that get transferred to the acceptor instead of the dye. The difference in amplitudes are however not as big as for the co-sensitized TiO_2-films. Due to the higher electron mobility in SnO_2 than in TiO_2, the electron transfer to the acceptor was expected to be faster for the mixed system. This is also suggested from the faster recombination rate to the dye on SnO_2. The reason why we don't see this could be due to the lower driving force for the electron transfer between SnO_2-CoPPIX than between TiO_2-CoPPIX, see figure 4.7. There might also be many regions in the sample were the electrons don't take the path from D35-TiO_2-SnO_2-CoPPIX. For this to be efficient, the semiconductors needs be placed strategically with the dye in contact with only TiO_2 and the acceptor in contact with only SnO_2.

To confirm that the electrons reach CoPPIX in the TAS measurements it would be necessary to probe also the reduced CoPPIX at either 435 nm or 375, but the absorbance of the samples were too high there so it was not possible to get any of that probe light to reach the detector.

4.4.4. Short summary

The charge separated state is longer lived in MeCN than in DMSO. The recombination rate is similar on the TiO_2/SnO2-films and the TiO_2-films and the fastest recombination is seen on SnO_2. The incorporation of CoPPIX is what affects the recombination rate the most. This changes the amplitudes, making the slower component more dominant. Figure 4.19 summarize the TAS-measurements in MeCN+MeOH.

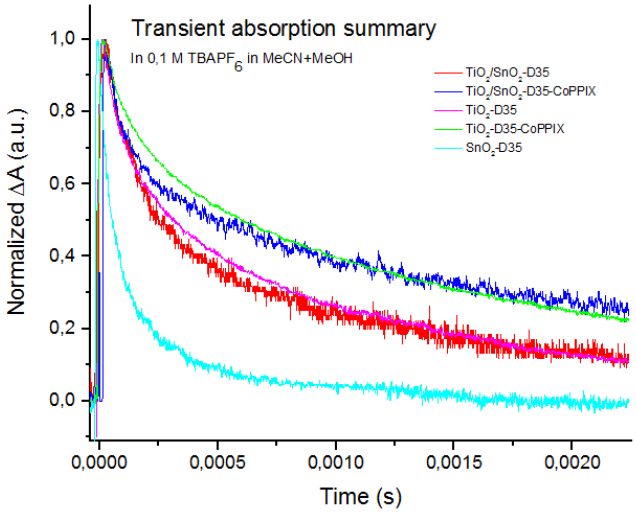

Figure 4.19. Summary of the TAS measurements in MeCN+MeOH

5. Conclusions and future outlook

In this project, conduction band mediated electron transfer across semiconductor thin films to CoPPIX, has been demonstrated. The CB-electrons can be used to reduce CoPPIX, suggesting that hybrid systems for solar fuel production is possible to use in the future.

The results from this project suggests that for a long lived charge separated state between the dye and the semiconductor, MeCN is a better solvent than DMSO. Adding MeOH to the solution does not affect the recombination rate much but it seems to make it a bit faster. However, for the CB mediated electron transfer, DMSO seems to be the best solvent. The lifetime of the charge separated state is longer for the TiO_2-films than for the SnO_2-films. When the atomic ratio of TiO_2/SnO_2 is 10/1 in the mixed films, the lifetime of the charge separated state is similar to the TiO_2-films. The recombination rate is affected the most by incorporating the acceptor molecule to the systems, this increases the lifetime of the excited state suggesting that electrons get transferred from the dye to the acceptor via the CB.

For future experiments it is crucial to improve the method for synthesizing the SnO_2-paste, so that more even films and comparable results can be obtained. The first try would be the hydrothermal method with a reactor that can withstand higher temperatures. A better way of mixing the pastes also needs to be looked into in order to mix them more evenly, probably the two pastes should be based on similar solvents.

The optimal solvent for the combined system is also something that needs to be further investigated before obtaining a working system. Perhaps MeCN could be a decent solvent for both processes if a coordinating molecule is added to the solution to facilitate the CB mediated electron transfer to CoPPIX.

For future experiments it would also be interesting to examine the effect of placing the semiconductors more strategically, so that the dye only is in contact with TiO_2 and that the acceptor only is in contact with SnO_2. That would make the electron transfer cascade more selective and effective. In the future it would also be necessary to look at more selective catalysts as acceptor molecules so that these systems could use the sunlight to reduce CO_2 into a higher value fuel.

6. Acknowledgments

First, I would like to thank Maria for allowing me to be part of her research group, letting me work with this interesting project and for all the help and support during the project. I would also like to thank Valeria for proposing this project, all the help in the lab, the support throughout the project and for the patience with answering all the questions that has come up during the project. The project would not have been the same without the two of you.

Thanks to Jimmy, whom I made the semiconductor films together with, thanks for the collaboration and support in the lab, the discussions and for all the funny moments.

I would also like to thank Damir, Jens, Victor and Joachim for helping out with the lasers. Thanks also to Rita and Pegah for the help in the lab. Thanks also to Stefan Gustafson for helping us with the SEM.

Thanks to the master thesis workers for the company in the office, the fika breaks and the laughter.

References

1. Dahl S, Chorkendorff I. Solar-fuel generation: towards practical implementation. Nature materials. 2012;11(2):100-1.
2. Hammarström L. Accumulative Charge Separation for Solar Fuels Production: Coupling Light-Induced Single Electron Transfer to Multielectron Catalysis. Accounts of chemical research. 2015;48(3):840-50.
3. Khan MA, Khan MZ, Zaman K, Naz L. Global estimates of energy consumption and greenhouse gas emissions. Renewable and Sustainable Energy Reviews. 2014;29:336-44.
4. Sahara G, Ishitani O. Efficient Photocatalysts for CO2 Reduction. Inorganic chemistry. 2015.
5. Benson EE, Kubiak CP, Sathrum AJ, Smieja JM. Electrocatalytic and homogeneous approaches to conversion of CO 2 to liquid fuels. Chemical Society Reviews. 2009;38(1):89-99.
6. Schneider J, Jia H, Muckerman JT, Fujita E. Thermodynamics and kinetics of CO2, CO, and H+ binding to the metal centre of CO2 reduction catalysts. Chemical Society Reviews. 2012;41(6):2036-51.
7. Gust D, Moore TA, Moore AL. Solar fuels via artificial photosynthesis. Accounts of chemical research. 2009;42(12):1890-8.
8. Morris AJ, Meyer GJ, Fujita E. Molecular approaches to the photocatalytic reduction of carbon dioxide for solar fuels. Accounts of chemical research. 2009;42(12):1983-94.
9. Grätzel M. Photoelectrochemical cells. Nature. 2001;414(6861):338-44.
10. Saavedra Becerril V. Studies of Charge Separation in Molecular and Molecular-Inorganic Materials Assemblies for Solar Energy Conversion. 2015.
11. Gust D, Moore TA, Moore AL. Molecular mimicry of photosynthetic energy and electron transfer. Accounts of chemical research. 1993;26(4):198-205.
12. Hayashi H, Lightcap IV, Tsujimoto M, Takano M, Umeyama T, Kamat PV, et al. Electron transfer cascade by organic/inorganic ternary composites of porphyrin, zinc oxide nanoparticles, and reduced graphene oxide on a tin oxide electrode that exhibits efficient photocurrent generation. Journal of the American Chemical Society. 2011;133(20):7684-7.
13. Clifford JN, Palomares E, Nazeeruddin MK, Thampi R, Grätzel M, Durrant JR. Multistep electron transfer processes on dye co-sensitized nanocrystalline TiO2 films. Journal of the American Chemical Society. 2004;126(18):5670-1.
14. Atkins PW, De Paula J, Friedman RS. Quanta, matter, and change: a molecular approach to physical chemistry. Oxford;New York;: Oxford University Press; 2009.
15. Lakowicz JR. Principles of fluorescence spectroscopy. New York: Springer; 2006.
16. Ceroni P, SpringerLink. The exploration of supramolecular systems and nanostructures by photochemical techniques. Dordrecht [Netherlands];New York;: Springer Verlag; 2012.
17. Hollas JM. Modern spectroscopy. Chichester: Wiley; 2004.
18. Smart L, Moore E. Solid state chemistry: an introduction. Boca Raton: CRC Press; 2012.
19. Bach U, Lupo D, Comte P, Moser J, Weissörtel F, Salbeck J, et al. Solid-state dye-sensitized mesoporous TiO2 solar cells with high photon-to-electron conversion efficiencies. Nature. 1998;395(6702):583-5.
20. Wiberg J, Marinado T, Hagberg DP, Sun L, Hagfeldt A, Albinsson B. Effect of anchoring group on electron injection and recombination dynamics in organic dye-sensitized solar cells. The Journal of Physical Chemistry C. 2009;113(9):3881-6.
21. Juozapavicius M, Kaucikas M, van Thor JJ, O'Regan BC. Observation of multiexponential pico-to subnanosecond electron injection in optimized dye-sensitized solar cells with visible-pump mid-infrared-probe transient absorption spectroscopy. The Journal of Physical Chemistry C. 2012;117(1):116-23.
22. Grätzel M. Solar energy conversion by dye-sensitized photovoltaic cells. Inorganic chemistry. 2005;44(20):6841-51.
23. Gregg BA, Pichot F, Ferrere S, Fields CL. Interfacial recombination processes in dye-sensitized solar cells and methods to passivate the interfaces. The Journal of Physical Chemistry B. 2001;105(7):1422-9.
24. Fujishima A, Zhang X, Tryk DA. TiO 2 photocatalysis and related surface phenomena. Surface Science Reports. 2008;63(12):515-82.
25. Reyes-Coronado D, Rodríguez-Gattorno G, Espinosa-Pesqueira M, Cab C, De Coss R, Oskam G. Phase-pure TiO2 nanoparticles: anatase, brookite and rutile. Nanotechnology. 2008;19(14):145605.
26. Shinde DV, Mane RS, Oh I-H, Lee JK, Han S-H. SnO 2 nanowall-arrays coated with rutile-TiO 2 nanoneedles for high performance dye-sensitized solar cells. Dalton Transactions. 2012;41(34):10161-3.
27. Vinodgopal K, Bedja I, Kamat PV. Nanostructured semiconductor films for photocatalysis. Photoelectrochemical behavior of SnO2/TiO2 composite systems and its role in photocatalytic degradation of a textile azo dye. Chemistry of materials. 1996;8(8):2180-7.
28. Green AN, Palomares E, Haque SA, Kroon JM, Durrant JR. Charge transport versus recombination in dye-sensitized solar cells employing nanocrystalline TiO2 and SnO2 films. The Journal of Physical Chemistry B. 2005;109(25):12525-33.
29. Staniszewski A, Morris AJ, Ito T, Meyer GJ. Conduction band mediated electron transfer across nanocrystalline TiO2 surfaces. The Journal of Physical Chemistry B. 2007;111(24):6822-8.

30. Tiwana P, Docampo P, Johnston MB, Snaith HJ, Herz LM. Electron mobility and injection dynamics in mesoporous ZnO, SnO2, and TiO2 films used in dye-sensitized solar cells. ACS nano. 2011;5(6):5158-66.
31. Song E, Shi C, Anson FC. Comparison of the behavior of several cobalt porphyrins as electrocatalysts for the reduction of O2 at graphite electrodes. Langmuir. 1998;14(15):4315-21.
32. Shen J, Kortlever R, Kas R, Birdja YY, Diaz-Morales O, Kwon Y, et al. Electrocatalytic reduction of carbon dioxide to carbon monoxide and methane at an immobilized cobalt protoporphyrin. Nature communications. 2015;6.
33. Ambrosio F, Martsinovich N, Troisi A. What is the best anchoring group for a dye in a dye-sensitized solar cell? The journal of physical chemistry letters. 2012;3(11):1531-5.
34. Dolphin D. The Porphyrins: Academic Press; 2012.
35. Ardo S, Achey D, Morris AJ, Abrahamsson M, Meyer GJ. Non-Nernstian Two-Electron Transfer Photocatalysis at Metalloporphyrin–TiO2 Interfaces. Journal of the American Chemical Society. 2011;133(41):16572-80.
36. Zaccheroni N. Spectrophotometry, Measurements in Solution. In: Ceroni P, editor. The Exploration of Supramolecular Systems and Nanostructures by Photochemical Techniques. Dordrecht: Springer Netherlands; 2012. p. 39-66.
37. Chappel S, Zaban A. Nanoporous SnO 2 electrodes for dye-sensitized solar cells: improved cell performance by the synthesis of 18nm SnO 2 colloids. Solar Energy Materials and Solar Cells. 2002;71(2):141-52.
38. Monti S, Chiorboli C. Transient Absorption Spectroscopy. In: Ceroni P, editor. The Exploration of Supramolecular Systems and Nanostructures by Photochemical Techniques. Dordrecht: Springer Netherlands; 2012. p. 185-207.
39. Mabbott GA. An introduction to cyclic voltammetry. Journal of Chemical education. 1983;60(9):697.
40. Kaim W, Fiedler J. Spectroelectrochemistry: the best of two worlds. Chemical Society Reviews. 2009;38(12):3373-82.
41. Yang L, Cappel UB, Unger EL, Karlsson M, Karlsson KM, Gabrielsson E, et al. Comparing spiro-OMeTAD and P3HT hole conductors in efficient solid state dye-sensitized solar cells. Physical Chemistry Chemical Physics. 2012;14(2):779-89.
42. Wang Q, Zakeeruddin SM, Nazeeruddin MK, Humphry-Baker R, Grätzel M. Molecular wiring of nanocrystals: NCS-enhanced cross-surface charge transfer in self-assembled Ru-complex monolayer on mesoscopic oxide films. Journal of the American Chemical Society. 2006;128(13):4446-52.
43. Selbin J, Bull W, Holmes L. Metallic complexes of dimethylsulphoxide. Journal of Inorganic and Nuclear Chemistry. 1961;16(3):219-24.

Appendix A

Below is the images and tables obtained from the EDX-analysis of the TiO_2/SnO_2-film.

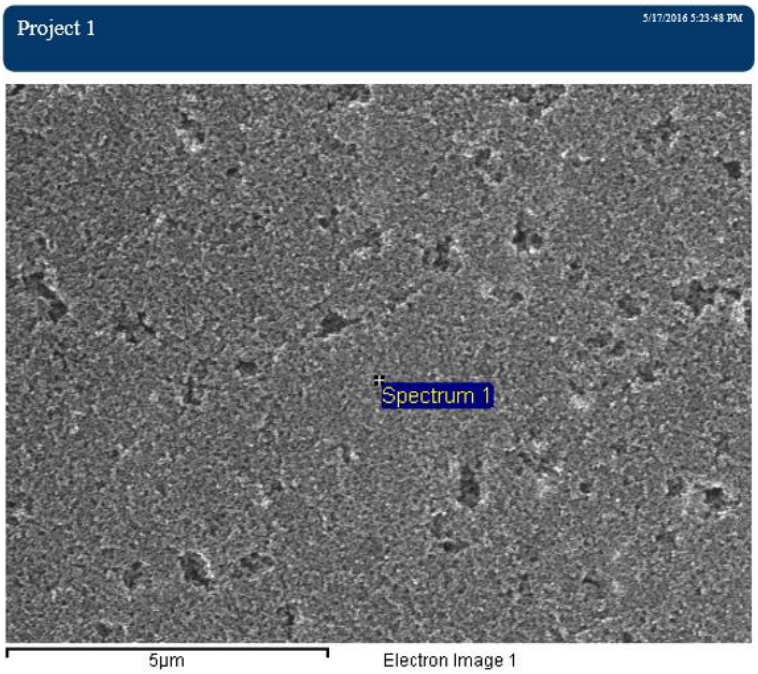

Processing option : All elements analysed (Normalised)

Spectrum	In stats.	O	Ti	Sn
Spectrum 1	Yes	71.07	26.55	2.38
Mean		71.07	26.55	2.38
Std. deviation		0.00	0.00	0.00
Max.		71.07	26.55	2.38
Min.		71.07	26.55	2.38

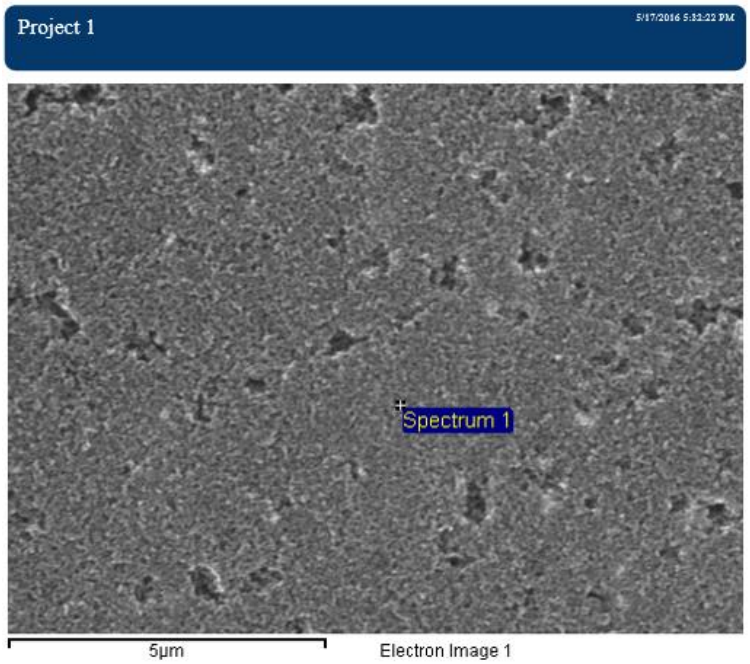

Processing option : All elements analysed (Normalised)

Spectrum	In stats.	O	Ti	Sn
Spectrum 1	Yes	71.07	26.55	2.38
Mean		71.07	26.55	2.38
Std. deviation		0.00	0.00	0.00
Max.		71.07	26.55	2.38
Min.		71.07	26.55	2.38

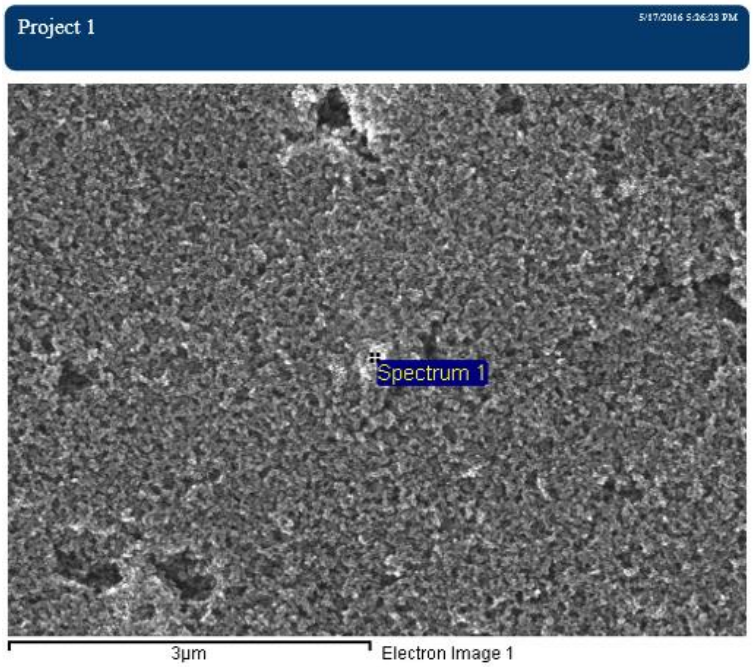

Processing option : All elements analysed (Normalised)

Spectrum	In stats.	O	Ti	Sn
Spectrum 1	Yes	69.71	27.67	2.62
Mean		69.71	27.67	2.62
Std. deviation		0.00	0.00	0.00
Max.		69.71	27.67	2.62
Min.		69.71	27.67	2.62

Appendix B

Figure B1 and B2 below shows the autoreduction of CoPPIX on TiO_2 and SnO_2 respectively. As can be seen there is a small auotreduction in both cases but not comparable to when UV-light is illuminating the film or when a negative potential is applied.

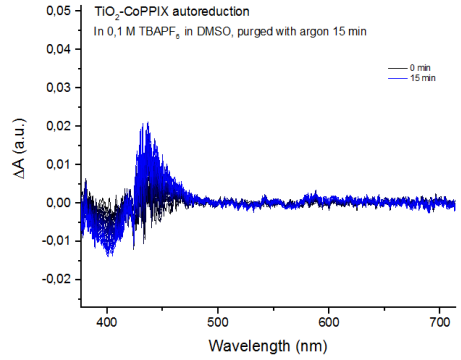

Figure B1. Differential spectrum of a TiO_2-CoPPIX-film in 0,1 MTBAPF$_6$ in DMSO with a few drops of MeOH as sacrificial donor (argon purged for 15 min) The spectrum is recorded every 30 seconds.

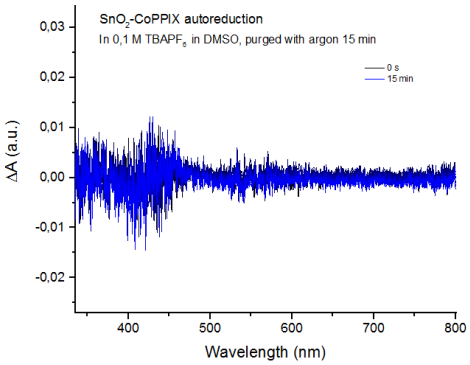

Figure B2. Differential spectrum of a SnO_2-CoPPIX-film in 0,1 MTBAPF$_6$ in DMSO with a few drops of MeOH as sacrificial donor (argon purged for 15 min) The spectrum is recorded every 30 seconds.

In figure B3 the spectrum obtained from illuminating a solution of CoPPIX with UV-light is shown. The same shift as when CoPPIX is reduced is not observed.

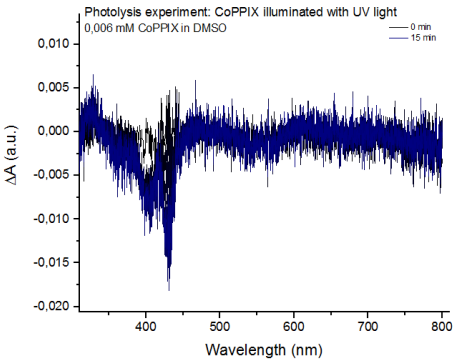

Figur B3. Differential spectrum of a 0.006 mM CoPPIX in 0,1 MTBAPF$_6$ in DMSO with a few drops of MeOH as sacrificial donor (argon purged for 15 min) The spectrum is recorded every 30 seconds.